Eur. Phys. J. B (2015) 88: 122
DOI: 10.1140/epjb/e2015-60213-4

THE EUROPEAN PHYSICAL JOURNAL B

Regular Article

Finite temperature effective field theory and two-band superfluidity in Fermi gases

Serghei N. Klimin[1,a], Jacques Tempere[1,2], Giovanni Lombardi[1], and Jozef T. Devreese[1,3]

[1] TQC, Universiteit Antwerpen, Universiteitsplein 1, 2610 Antwerpen, Belgium
[2] Lyman Laboratory of Physics, Harvard University, Cambridge, MA 02138, USA
[3] Technische Universiteit Eindhoven, Eindhoven, The Netherlands

Received 16 March 2015 / Received in final form 8 April 2015
Published online 11 May 2015 –

Abstract. We develop a description of fermionic superfluids in terms of an effective field theory for the pairing order parameter. Our effective field theory improves on the existing Ginzburg-Landau theory for superfluid Fermi gases in that it is not restricted to temperatures close to the critical temperature. This is achieved by taking into account long-range fluctuations to all orders. The results of the present effective field theory compare well with the results obtained in the framework of the Bogoliubov-de Gennes method. The advantage of an effective field theory over Bogoliubov-de Gennes calculations is that much less computation time is required. In the second part of the paper, we extend the effective field theory to the case of a two-band superfluid. The present theory allows us to reveal the presence of two healing lengths in the two-band superfluids, to analyze the finite-temperature vortex structure in the BEC-BCS crossover, and to obtain the ground state parameters and spectra of collective excitations. For the Leggett mode our treatment provides an interpretation of the observation of this mode in two-band superconductors.

1 Introduction

Multi-bandgap superconductivity, predicted by Suhl et al. [1], was first revealed in MgB_2 [2,3], and more recently in the iron pnictide class of superconductors [4]. The multiple bandgaps arise from differences in character between the Fermi surface sheets on which Cooper pairing takes place [3]. In the two-bandgap superconductor MgB_2, the two Cooper pairing channels moreover appear to be in different regimes: taken individually they would lead to type I and type II superconductivity, respectively. Therefore, this material was dubbed a "type 1.5" superconductor [5]. The competing length scales associated with the Cooper pairing channels lead to the formation of vortex clusters and stripes [5,6]. The experimental discovery of vortex clustering in MgB_2 has lead to a flurry of activity to develop a two-bandgap Ginzburg-Landau (GL) formalism suitable to describe these patterns.

The increasing interest in two-band superfluid fermionic system is not restricted to superconductors [7]. Recently, the superfluidity of multiband ultracold atomic Fermi gases has attracted theoretical attention [8–10], anticipating interesting experiments in this field. Quantum gases offer the singular advantage that the adaptability of various experimental parameters (intraband and interband interaction strength, numbers of atoms, trapping geometry,...) allows to study these systems in regimes inaccessible in solids. A GL theory has been developed for these systems at the microscopic level [10–12], as distinct from the case of superconductivity where many parameters remain phenomenological. Here, we focus on two-bandgap superfluidity in atomic Fermi gases throughout the crossover from the weak-coupling BCS regime to the Bose-Einstein condensate (BEC) regime, where pairing of molecules in real space occurs.

In the straightforward two-component GL expansion (TCGL) two single-component GL equations are coupled through a Josephson term (see, e.g. Refs. [13–15]), and lead to an intervortex interaction that can account for vortex clustering [16]. However, the validity of this simple extension has been the subject of intense debate [17–23]. Kogan and Schmalian [17,19] indicate that the two order parameters in a two-band superconductor should have the same length scale of spatial variation in the vicinity of the critical temperature T_c, when $T \to T_c$. Since the standard GL formalism is developed for T near T_c, these authors conclude that the GL approach fails to adequately describe the existence of two different length scales in a two-band superconductor. On the other hand, Babaev and Silaev [18] argue that the TCGL expansion is justified and properly describes two-band systems with different coherence lengths. Both sides, however, recognize that the temperature range of validity for the TCGL approach is restricted from below by the condition that the order parameter amplitude is small [23]. Therefore, finding an effective TCGL-like formalism valid well below T_c remains

[a] e-mail: sergei.klimin@uantwerpen.be

an open question. In references [20,21,24,25], an extended two-component GL formalism is found by performing an expansion of the free energy and the gap equation in powers of $\tau = 1 - T/T_c$ to order $\tau^{3/2}$ rather than $\tau^{1/2}$ as is common for the standard GL formalism. This approach confirms the existence of two distinct length scales [26]. However in practice a complete summation of the series over τ is not feasible.

It was shown [23] that a TCGL model with phenomenologically determined coefficients yields an accurate description of vortices and of the magnetic response of a two-band superconductor in a wide range of temperatures. Models where the GL parameters are calculated from a microscopic theory are available in the limit of weak-coupling BCS superconductors (e.g. Refs. [27,28]), where the assumption of slowly varying fields was a key ingredient. Here, we invoke the same assumption to develop a theory that avoids any additional approximation (for example, small τ, small pair field, or weak coupling) and that retrieves in limiting cases the results of known effective field theories. Our finite-temperature effective field theory retrieves the zero-temperature effective field theory [29,30] in the limit $T \to 0$ throughout the BCS-BEC crossover. Also in the other limit, $T \to T_c$, the obtained EFT analytically reproduces the results obtained by the microscopic path-integral treatment for the homogeneous superfluid in the entire BCS-BEC crossover [11,12]. The effective field theory that we obtain in this way has been applied successfully to dark solitons in ultracold Fermi gases [31], where it shows a good agreement with Bogoliubov-de Gennes theory. The present work for the first time systematically describes the derivation of the finite temperature EFT formalism, which is only briefly represented in reference [31], and applies the theory to describe vortex structure in the BCS-BEC crossover.

Next, we extend the effective field theory to interacting mixtures of superfluid Fermi gases. When two pairing channels are available, these systems represent the quantum gas analog of the two-band superconductors discussed above. Specifying the species of trapped atoms, their hyperfine states, and the number of trapped atoms, fixes unambiguously the microscopic Hamiltonian in terms of scattering lengths, chemical potentials, and masses. Starting from the microscopic action functional for two-band atomic Fermi gases with s-wave pairing, we obtain unique expressions for the parameters of the effective field theory for the two band superfluid, including expressions for the Josephson coupling between the two order parameters as a function of the scattering lengths. The resulting effective field theory reveals the presence of two healing length scales in the two-band superfluids, in close analogy to the so-called hidden criticality discussed for two-band superconductors. In order for the theory to be capable of describing the experimentally relevant collective excitations of superfluid Fermi gases, a derivative expansion keeping only the first order derivatives of the pair field over time (performed, e.g. in Refs. [11,12]) is not sufficient: second-order time derivatives are required to determine collective excitation spectra of Fermi superfluids. Including these second-order derivatives, we obtain the collective modes including the Leggett mode, and compare the results obtained in the framework of superfluid two-band systems to experimental results obtained for the Leggett mode in two-band superconductors.

The paper is divided in two parts. In the first part, Section 2, we derive the effective field action and the field equations for a single-component Fermi superfluid (Sect. 2.1). In this part we also compare the results for the thermodynamics of the uniform system to the results of the microscopic description to show the validity of the field theory for a large temperature range in Section 2.2. Also the structure of a vortex in the BCS-BEC crossover (Sect. 2.3), as well as the collective excitation spectrum (Sect. 2.4) are calculated and compared to existing treatments such as the Bogoliubov-de Gennes treatment. In the second part (Sect. 3), we extend the results to a two-band system (Sect. 3.1), and consider the behavior of the parameters and thermodynamic quantities of two-band superfluid Fermi gases at zero temperature and at finite temperatures (Sect. 3.2). The spectra of collective excitations are again calculated (Sect. 3.3), revealing for the two-band case also the Leggett mode, i.e. the out-of-phase oscillation mode between the two bands. The discussion is summarized in Section 4.

2 Effective field theory for superfluid Fermi gases

2.1 Derivation of the field equations

2.1.1 Functional integral formalism

An effective field theory for the superfluid order parameter constitutes a powerful tool to study non-uniform phenomena in fermionic superfluids, such as vortices, solitons, and the effects of strong confinement. Examples are the Gross-Pitaevskii equation for the temperature-zero Bose gas and the Ginzburg-Landau theory for superconductors near the critical temperature. These approaches are complementary to microscopic descriptions such as the Bogoliubov-de Gennes approach. The latter works well for small number of particles, whereas a description in terms of an effective field theory meets no difficulties for large numbers of particles, including the thermodynamic limit. The other advantage of an effective-field based description is that this usually requires much less computation time and memory than the Bogoliubov-de Gennes calculation. Up to now, Ginzburg-Landau (GL) type effective field theories have been developed for superfluid Fermi gases at $T \approx T_c$ [11,12] or at $T = 0$ [29,30]. Both assume a slow variation of a pair field in space and time, and account for amplitude as well as phase field fluctuations. For the two-dimensional Fermi superfluid, a finite-temperature effective field theory has been formulated taking into account phase fluctuations in 2D [32,33]. An effective field theory for cold Fermi gases in 3D has been derived within the mean-field approximation [34]. The goal of the first part

of the present paper is to develop an effective field theory that is valid in the whole temperature range up to T_c and accounts for both amplitude and phase of the pair field *without assuming fluctuations small*. This extension in performed within the functional integral formalism used in reference [11] and in subsequent works. No additional hypotheses or modelling are introduced.

We consider a fermionic system of particles with two spin states each ($\sigma = \uparrow, \downarrow$). In the functional integral formalism, the partition function of the fermionic system is determined by the path integral over the fermion fields (the Grassmann variables):

$$\mathcal{Z} \propto \int \mathcal{D}\left[\bar{\psi}, \psi\right] e^{-S}. \tag{1}$$

The system is described by the action functional S of the fermionic fields ψ_σ, which is given by:

$$S = S_0 + \int_0^\beta d\tau \int d\mathbf{r}\, U(\mathbf{r}, \tau), \tag{2}$$

where $\beta = 1/(k_B T)$, T is the temperature, k_B is the Boltzmann constant, and S_0 is the free-fermion action,

$$S_0 = \int_0^\beta d\tau \int d\mathbf{r} \sum_{\sigma=\uparrow,\downarrow} \bar{\psi}_\sigma \left(\frac{\partial}{\partial \tau} + H_\sigma\right) \psi_\sigma. \tag{3}$$

The one-particle Hamiltonian $H_\sigma = -\nabla_{\mathbf{r}}^2/(2m) - \mu_\sigma$ allows for population imbalance through the chemical potentials μ_σ. The interaction Hamiltonian $U(\mathbf{r}, \tau)$ describes the contact interactions between fermions:

$$U = g\bar{\psi}_\uparrow \bar{\psi}_\downarrow \psi_\downarrow \psi_\uparrow. \tag{4}$$

The interaction energy with the coupling constant g is determined by the s-wave scattering between two fermions with antiparallel spins: this is the Cooper pairing channel. We use the following set of units: $\hbar = 1$, $m = 1/2$, and the Fermi energy for a free-particle Fermi gas $E_F \equiv \hbar^2 k_F^2/(2m) = 1$, where $k_F \equiv \left(3\pi^2 n\right)^{1/3}$ is the Fermi wave vector and n is the fermion particle density. The antisymmetry requirement for fermionic wave functions prohibits s-wave scattering between fermions with parallel spin.

The Hubbard-Stratonovich (HS) transformation is based on introducing bosonic fields $\bar{\Psi}, \Psi$ such that the partition function is represented through the path integral over the Fermi and Bose fields,

$$\mathcal{Z} \propto \int \mathcal{D}\left[\bar{\psi}, \psi\right] \int \mathcal{D}\left[\bar{\Psi}, \Psi\right] e^{-S_{HS}}. \tag{5}$$

The HS action which exactly decouples the four-field interaction terms in the initial Hamiltonian, is the same as in reference [11],

$$S_{HS} = S_0 + S_B + \int_0^\beta d\tau \int d\mathbf{r} \left(\bar{\Psi}\psi_\uparrow \psi_\downarrow + \Psi \bar{\psi}_\downarrow \bar{\psi}_\uparrow\right), \tag{6}$$

with the free-boson action

$$S_B = -\int_0^\beta d\tau \int d\mathbf{r}\, \frac{1}{g} \bar{\Psi}\Psi. \tag{7}$$

In order to address the whole range of the BCS-BEC crossover, the coupling constant g is renormalized through the s-wave scattering length a_s exactly as in reference [11] for the one-band system:

$$\frac{1}{g} = m\left(\frac{1}{4\pi a_s} - \int_{k<K} \frac{d\mathbf{k}}{(2\pi)^3} \frac{1}{k^2}\right), \tag{8}$$

with the ultraviolet cutoff $K \to \infty$. The integration over the fermion fields leads to the partition function,

$$\mathcal{Z} \propto \int \mathcal{D}\left[\bar{\Psi}, \Psi\right] e^{-S_{\text{eff}}}, \tag{9}$$

with the effective bosonic action S_{eff} depending on the pair field only:

$$S_{\text{eff}} = S_B - \operatorname{Tr} \ln\left[-\mathbb{G}^{-1}\right]. \tag{10}$$

Here $\mathbb{G}^{-1}(\mathbf{r}, \tau) = \mathbb{G}_0^{-1}(\mathbf{r}, \tau) - \mathbb{F}(\mathbf{r}, \tau)$ is the inverse Nambu tensor, written as a sum of the free-fermion inverse Nambu tensor $\mathbb{G}_0^{-1}$ and the matrix $\mathbb{F}$ proportional to the pair field Ψ:

$$\mathbb{G}_0^{-1}(\mathbf{r}, \tau) = \begin{pmatrix} -\frac{\partial}{\partial \tau} - \hat{H}_\uparrow & 0 \\ 0 & -\frac{\partial}{\partial \tau} + \hat{H}_\downarrow \end{pmatrix}, \tag{11}$$

$$\mathbb{F}(\mathbf{r}, \tau) = \begin{pmatrix} 0 & -\Psi(\mathbf{r}, \tau) \\ -\bar{\Psi}(\mathbf{r}, \tau) & 0 \end{pmatrix}. \tag{12}$$

The effective action (10) is expanded as a series in powers of the pair field:

$$S_{\text{eff}} = S_B - \operatorname{Tr} \ln\left[-\mathbb{G}_0^{-1}\right] + \sum_{p=1}^{\infty} \frac{1}{p} \operatorname{Tr}\left[(\mathbb{G}_0 \mathbb{F})^p\right]. \tag{13}$$

As the integration over the bosonic fields cannot be performed analytically for the effective action (13), approximations are necessary.

2.1.2 Gradient expansion

The crudest approximation would be to assume the pair field to be constant in space and time, $\Psi(\mathbf{r}, \tau) = |\Psi|$, so that $\mathbb{F}(\mathbf{r}, \tau) = \mathbb{F}(\mathbf{r}_0, \tau_0) = \mathbb{F}_0$ is independent of space and time. This is the saddle-point approximation, and it corresponds to replacing all factors $\mathbb{F}$ in $(\mathbb{G}_0 \mathbb{F})^p$ by the constant $\mathbb{F}_0$. Then, the sum over all orders of p in expression (13) can be performed analytically. One readily obtains the saddle point action, and the corresponding saddle point free energy

$$\Omega_s(w) = -\int \frac{d\mathbf{k}}{(2\pi)^3} \left(\frac{1}{\beta} \ln\left(2\cosh \beta E_{\mathbf{k}} + 2\cosh \beta\zeta\right) - \xi_{\mathbf{k}} - \frac{w}{2k^2}\right) - \frac{w}{8\pi a_s}, \tag{14}$$

with $w = |\Psi|^2$. Here, $E_{\mathbf{k}} = \sqrt{\xi_{\mathbf{k}}^2 + w}$ is the Bogoliubov excitation energy, and $\xi_{\mathbf{k}} = k^2 - \mu$ is the free-fermion energy. The chemical potentials for the imbalanced fermions are expressed as $\mu_\uparrow = \mu + \zeta$ and $\mu_\downarrow = \mu - \zeta$.

To improve on the saddle-point approximation, Gaussian pair fluctuations can be taken into account. Then, one writes $\Psi(\mathbf{r}, \tau) = |\Psi| + \delta\Psi$ with corresponding $\mathbb{F}(\mathbf{r}, \tau) = \mathbb{F}_0 + \delta\mathbb{F}(\mathbf{r}, \tau)$, and expands the action functional up to second order in the small parameter $\delta\Psi$. This is equivalent to truncating the sum over p in expression (13) at $p = 2$. This restricted sum leads to gaussian path integrals which can be performed analytically [11,12,29,30].

In the present work, we go beyond this limitation, and again take the sum over all powers of p. To do this, we assume that the pair field varies slowly in space and time, so we can expand the matrix $\mathbb{F}$ around its background value

$$\mathbb{F}(\mathbf{r}, \tau) = \mathbb{F}_0 + \partial_\tau \mathbb{F}|_0 (\tau - \tau_0) + \nabla \mathbb{F}|_0 \cdot (\mathbf{r} - \mathbf{r}_0) + \dots \quad (15)$$

taking also second derivatives (not written down here) into account. Subsequently, we replace all but (at most) two factors $\mathbb{F}$ in $(\mathbb{G}_0\mathbb{F})^p$ by $\mathbb{F}_0$. The remaining factors $\mathbb{F}$ in $(\mathbb{G}_0\mathbb{F})^p$ are then expanded according to (15). Since the coefficients $.\nabla\mathbb{F}|_0$, $.\partial_\tau\mathbb{F}|_0$,... are constant, we find that the trace of $(\mathbb{G}_0\mathbb{F})^p$ can be taken and summed over all p analytically. Thus, after the expansion of the action (13) in gradients, we perform the *complete* summation over p *analytically exactly*, without assuming $\mathbb{F}_0$ small. Correspondingly, the range of applicability of this derivative expansion is the same as for the Ginzburg-Landau approach as far as the spatial and temporal variations are concerned, but without assuming the "background" Ψ small. A similar scheme was developed in references [29,30] at $T = 0$ and in the unitarity regime. Here, we perform the complete summation of the series in powers of $\bar{\Psi}, \Psi$ at finite temperatures and at arbitrary coupling strengths.

2.1.3 Effective action functional

As a result, the effective bosonic action S_{eff} is approximated by the following effective field action S_{EFT}:

$$\begin{aligned} S_{EFT} = \int_0^\beta d\tau \int d\mathbf{r} \Bigg\{ \Bigg[& \Omega_s(w) + \frac{\mathcal{D}(w)}{2} \\ & \times \left(\bar{\Psi}\frac{\partial\Psi}{\partial\tau} - \frac{\partial\bar{\Psi}}{\partial\tau}\Psi \right) + \tilde{\mathcal{Q}}(w) \frac{\partial\bar{\Psi}}{\partial\tau}\frac{\partial\Psi}{\partial\tau} \\ & - \frac{\mathcal{R}(w)}{2w}\left(\frac{\partial w}{\partial\tau}\right)^2 + \frac{\tilde{\mathcal{C}}(w)}{2m}\left(\nabla_{\mathbf{r}}\bar{\Psi}\cdot\nabla_{\mathbf{r}}\Psi\right) \\ & - \frac{\mathcal{E}(w)}{2mw}\left(\nabla_{\mathbf{r}} w\right)^2 \Bigg] \Bigg\}. \end{aligned} \quad (16)$$

The (local) saddle-point thermodynamic potential is still determined by the modulus squared of the position-dependent order parameter, $w = |\Psi|^2$ as in expression (14). The other coefficients are given by:

$$\tilde{\mathcal{C}} = \int \frac{d\mathbf{k}}{(2\pi)^3}\frac{k^2}{3m} f_2(\beta, E_{\mathbf{k}}, \zeta), \quad (17)$$

$$\mathcal{D} = \int \frac{d\mathbf{k}}{(2\pi)^3}\frac{\xi_{\mathbf{k}}}{w}\left[f_1(\beta, \xi_{\mathbf{k}}, \zeta) - f_1(\beta, E_{\mathbf{k}}, \zeta)\right], \quad (18)$$

$$\mathcal{E} = 2w\int \frac{d\mathbf{k}}{(2\pi)^3}\frac{k^2}{3m}\xi_{\mathbf{k}}^2\, f_4(\beta, E_{\mathbf{k}}, \zeta), \quad (19)$$

$$\begin{aligned} \tilde{\mathcal{Q}} = \frac{1}{2w}\int \frac{d\mathbf{k}}{(2\pi)^3} & \left[f_1(\beta, \xi_{\mathbf{k}}, \zeta)\right. \\ & \left. - \left(E_{\mathbf{k}}^2 + \xi_{\mathbf{k}}^2\right) f_2(\beta, E_{\mathbf{k}}, \zeta)\right], \end{aligned} \quad (20)$$

$$\begin{aligned} \mathcal{R} = \int \frac{d\mathbf{k}}{(2\pi)^3} & \left[\frac{f_1(\beta, \xi_{\mathbf{k}}, \zeta) + \left(E_{\mathbf{k}}^2 - 3\xi_{\mathbf{k}}^2\right) f_2(\beta, \xi_{\mathbf{k}}, \zeta)}{3w}\right. \\ & \left. + \frac{4\left(\xi_{\mathbf{k}}^2 - 2E_{\mathbf{k}}^2\right)}{3} f_3(\beta, \xi_{\mathbf{k}}, \zeta) + 2E_{\mathbf{k}}^2 w f_4(\beta, \xi_{\mathbf{k}}, \zeta)\right]. \end{aligned} \quad (21)$$

The functions $f_p(\beta, \varepsilon, \zeta)$ are determined explicitly using the recurrence relations:

$$f_1(\beta, \varepsilon, \zeta) = \frac{1}{2\varepsilon}\frac{\sinh(\beta\varepsilon)}{\cosh(\beta\varepsilon) + \cosh(\beta\zeta)}, \quad (22)$$

$$f_{p+1}(\beta, \varepsilon, \zeta) = -\frac{1}{2p\varepsilon}\frac{\partial f_p(\beta, \varepsilon, \zeta)}{\partial\varepsilon}. \quad (23)$$

The corresponding equations for the order parameter follow from the stationary action principle with the functional (16). In order to study the evolution of the order parameter in real time, we replace τ by it as in reference [11]. This results in a set of two coupled equations. The first equation reads:

$$\begin{aligned} i\frac{\partial(w\mathcal{D})}{\partial w}\frac{\partial\Psi}{\partial t} = {} & \mathcal{A}(w)\Psi + \mathcal{Q}\frac{\partial^2\Psi}{\partial t^2} - \frac{\mathcal{R}\Psi^2}{w}\frac{\partial^2\bar{\Psi}}{\partial t^2} \\ & - \frac{1}{w}\frac{\partial(w\mathcal{R})}{\partial w}\Psi\frac{\partial\bar{\Psi}}{\partial t}\frac{\partial\Psi}{\partial t} \end{aligned} \quad (24)$$

$$\begin{aligned} & + \left(\frac{\partial\mathcal{Q}}{\partial w} + \frac{1}{2w}\frac{\partial(w\mathcal{R})}{\partial w}\right)\bar{\Psi}\left(\frac{\partial\Psi}{\partial t}\right)^2 \\ & - \frac{1}{2}\frac{\partial\left(\frac{\mathcal{R}}{w}\right)}{\partial w}\Psi^3\left(\frac{\partial\bar{\Psi}}{\partial t}\right)^2 \end{aligned} \quad (25)$$

$$\begin{aligned} & - \mathcal{C}\nabla_{\mathbf{r}}^2\Psi + \frac{2\mathcal{E}\Psi^2}{w}\nabla_{\mathbf{r}}^2\bar{\Psi} \\ & + \frac{2}{w}\frac{\partial(w\mathcal{E})}{\partial w}\Psi\left(\nabla_{\mathbf{r}}\bar{\Psi}\cdot\nabla_{\mathbf{r}}\Psi\right) \\ & - \left(\frac{\partial\mathcal{C}}{\partial w} + \frac{1}{w}\frac{\partial(w\mathcal{E})}{\partial w}\right)\bar{\Psi}\left(\nabla_{\mathbf{r}}\Psi\right)^2 \\ & + \frac{\partial\left(\frac{\mathcal{E}}{w}\right)}{\partial w}\Psi^3\left(\nabla_{\mathbf{r}}\bar{\Psi}\right)^2, \end{aligned} \quad (26)$$

and the other equation is conjugate to (26). Here, the coefficients $\mathcal{C}$ and $\mathcal{Q}$ are related to, respectively, $\tilde{\mathcal{C}}$ and $\tilde{\mathcal{Q}}$ by:

$$\mathcal{C} = \tilde{\mathcal{C}} - 2\mathcal{E}, \quad \mathcal{Q} = \tilde{\mathcal{Q}} - \mathcal{R}. \quad (27)$$

The coefficient $\mathcal{A} \equiv \partial\Omega_s/\partial w$ is given by:

$$\mathcal{A}(w) = -\int \frac{d\mathbf{k}}{(2\pi)^3}\left(\frac{1}{2E_{\mathbf{k}}}\frac{\sinh(\beta E_{\mathbf{k}})}{\cosh(\beta E_{\mathbf{k}})+\cosh(\beta\zeta)} - \frac{1}{2k^2}\right) - \frac{1}{8\pi a_s}. \quad (28)$$

Note that within the local-density approximation (LDA) time and space derivatives in (26) are neglected, and we arrive at the known gap equation for a uniform Fermi superfluid

$$\mathcal{A}(w) = 0. \quad (29)$$

In the BCS-BEC crossover regime, the coefficient $\mathcal{E}$ in (26) is, in general, not negligible. This leads to mixing of Ψ and $\bar{\Psi}$ in the evolution equations. This mixing is not surprising. In the particular case when space and time variations of the order parameter about its saddle-point value $\delta\Psi \equiv \Psi - \Delta$ are small, these variations are equivalent to the Gaussian fluctuations [11]. For temperatures below T_c, the fluctuation action is a non-diagonal quadratic form: it contains terms which mix conjugate and non-conjugate pair fields [35].

Taking the limit $T \to T_c$ in the present approach and neglecting the second-order time derivatives, we can compare the effective field action of the present work with the results of the standard Ginzburg-Landau type theory [11,12]. In taking the $T \to T_c$ limit, we also expand the thermodynamic potential with respect to $w = |\Psi|^2$ up to quartic order in the pair field: $\Omega_s^{GL} = \Omega_s|_{w=0} - aw + bw^2/2$. The coefficients a and b obtained in this way coincide *exactly* with those given in reference [11]. However, performing the summations over p in (13) before taking the limit $w \to 0$ we find that the coefficient $\mathcal{D}$ differs from the coefficient d of reference [11]:

$$\lim_{w\to 0}\mathcal{D}(w) = \frac{1}{4}\int \frac{d\mathbf{k}}{(2\pi)^3}\left(\frac{\tanh\frac{\beta\xi_{\mathbf{k}}}{2}}{\xi_{\mathbf{k}}^2} - \frac{\beta}{2\xi_k\cosh^2\frac{\beta\xi_{\mathbf{k}}}{2}}\right). \quad (30)$$

It remains real for all $T < T_c$, whereas an imaginary part appears just when the order of limits $w \to 0$ and $T \to T_c$ is reversed. This difference is explained by the fact that in reference [11], $|\Psi|$ is a small parameter, so that the chemical potential μ plays the role of the energy scale. There is a point close to the unitarity regime where both μ and $|\Psi|$ turn to zero. In this singularity point, the energy scale vanishes and the time dependent Ginzburg Landau description (TDGL), as concluded in reference [11], fails. Contrary to the regime near T_c, a TDGL equation is obtained in reference [11] for all couplings at $T = 0$. In this case a nonzero order parameter "precludes a vanishing energy scale, and the low frequency expansion of the effective action is well defined for all couplings" [11]. In the present approach, $|\Psi|$ is *not* a small parameter, because we performed the summation of the effective field action over the whole series in powers of $|\Psi|$. Therefore the derived effective field action is valid not only for the zero temperature case but also for the whole range of temperatures below T_c, except, maybe, for a vicinity of the aforesaid singular point.

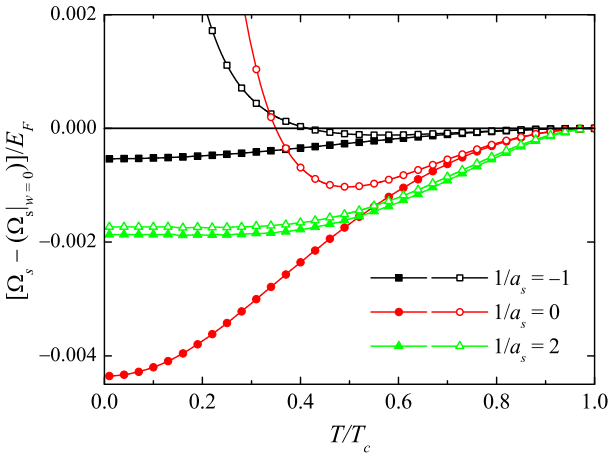

Fig. 1. Thermodynamic potential difference $\Omega_s - (\Omega_s|_{w=0})$ calculated within the finite temperature EFT (full symbols) and within the standard GL theory [11] (hollow symbols) as a function of the temperature for different values of the inverse scattering length.

The coefficient at the first time derivative obtained in the present work is verified by the comparison with the corresponding coefficient found in references [32,33] for a Fermi gas in 2D keeping only the phase fluctuations but without assuming the phase to be small. This confirms the importance of a correct sequence of limits: $T \to T_c$ and $|\Psi| \to 0$. When $|\Psi| = 0$ is set from the very beginning, as in reference [11], and then T varies, a singularity appears at $T = T_c$ and $\mu = 0$. On the contrary, the coefficient (30) contains no singularity when passing the point $\mu = 0$.

2.2 Thermodynamic potential

As established in references [36,37], for a BCS superconductor the dynamic part of the effective action must be, in general, time-nonlocal and contain both propagating and dissipative parts. In the weak-coupling BCS superconductors the propagating part is less than the damped one [38]. However, in the atomic Fermi gases, the propagating component plays an important role because of the presence of the condensed molecular bosons whose dynamics is primarily the conserved one [39]. The developed formalism catches the non-dissipative part of the time-dependent term in the effective action. Thus the evolution equation for the order parameter (when neglecting the second-order time derivatives) is governed by a time-dependent nonlinear Schrödinger equation [40,41] (rather than a time dependent Ginzburg-Landau equation, which must account for the carrier dissipation).

Figure 1 shows the difference $\Omega_s - (\Omega_s|_{w=0})$ as a function of temperature for several values of the inverse scattering length $1/a_s$, for the present approach (full curves) and the standard GL approach (dashed curves). According to the chosen system of units, a_s is measured in units of the inverse to the Fermi wave vector k_F, and Ω_s is measured in units of E_F. The same units are assumed in the other figures. As discussed in the previous paragraph,

near T_c the results are close to each other. For $T \to 0$, the present approach converges to the result for the ground state energy of the superfluid Fermi gas obtained in the microscopic theory of the homogeneous system. Indeed, in the limit of a stationary and homogeneous system without vortices, the minimization of the effective action (16) obviously leads to the saddle-point gap equation of reference [11] for all temperatures. In contrast, the standard GL approach is seen to fail for $T \ll T_c$, and does so more strongly for negative scattering lengths.

2.3 Finite-temperature vortex

Vortices in superfluid Fermi gases in the BCS-BEC crossover have been studied with several methods. The vortex core structure was elucidated within a Bogoliubov-de Gennes approach by Simonucci et al. [42]. The BdG results of reference [42] describe an isolated vortex beyond the weak-coupling BCS case, and in the whole temperature range $0 < T < T_c$. Also the present effective field theory allows us to investigate the vortex core structure at arbitrary temperature and coupling strengths, and has the advantage of requiring much less computational effort. Here, we compare the results from the present treatment to the BdG results.

In Figure 2, the amplitude modulation function $a(r) \equiv |\Psi(r)|/|\Psi(\infty)|$ for a vortex is plotted for several inverse scattering lengths $1/a_s$ and several temperatures. In reference [42], three temperatures are considered for each scattering length: $T/T_c = 0$, 0.5, and 0.9. We use the same temperatures, except $T = 0$: the low-temperature curves are calculated here for $T/T_F = 0.005$. At low temperatures the calculated results very slowly depend on T, so that we can compare our low-temperature results with those for $T = 0$ from reference [42]. We find that the agreement is good as the temperature becomes larger or the interaction regime goes towards the BEC regime. A significant quantitative difference between BdG and EFT appears only in the BCS regime at low temperatures.

In Figure 3, we plot the distributions of the total fermion density, comparing BdG and EFT results. The density can be calculated by two methods: (1) in the local density approximation (LDA):

$$n^{(\mathrm{LDA})} = -\frac{\partial \Omega_s}{\partial \mu}, \tag{31}$$

and (2) accounting for the gradient terms in the effective action (54),

$$n^{(tot)} = -\frac{\partial \Omega_s}{\partial \mu} - \frac{1}{2}\frac{\partial \rho_{qp}}{\partial \mu}\left(\frac{da\,(r)}{dr}\right)^2 - \frac{1}{2r^2}\frac{\partial \rho_{sf}}{\partial \mu}a^2\,(r) \tag{32}$$

with the superfluid density ρ_{sf} and the quantum pressure coefficient ρ_{qp}:

$$\rho_{sf} = \frac{\tilde{\mathcal{C}}}{m}\,|\Psi|^2\,, \tag{33}$$

$$\rho_{qp} = \frac{\left(\tilde{\mathcal{C}} - 4\mathcal{E}\right)\Delta^2}{m}. \tag{34}$$

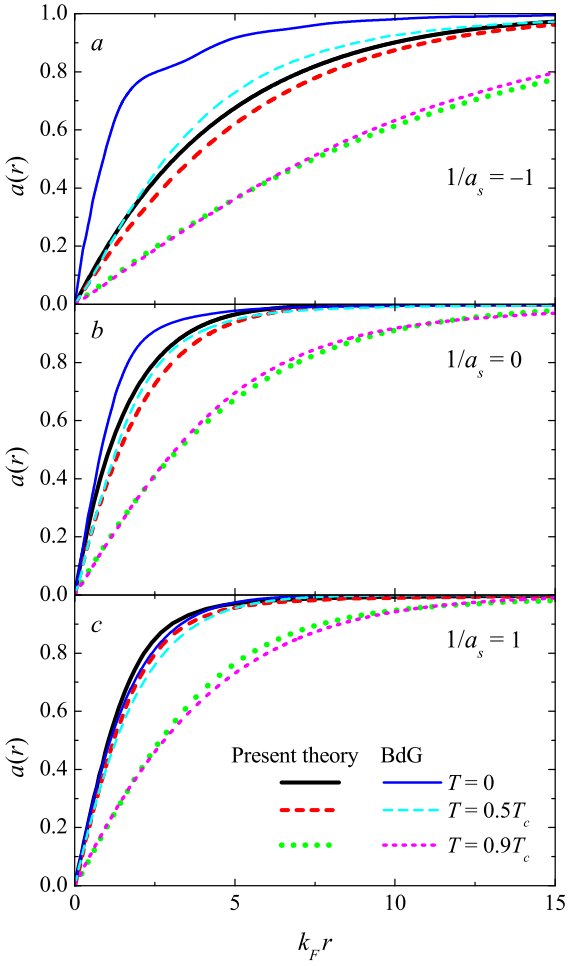

Fig. 2. Amplitude modulation function of the order parameter $a(r) = |\Psi(r)|/|\Psi(\infty)|$ for a vortex at different temperatures and scattering lengths. The results of the present theory (heavy curves) are compared with the BdG data of reference [42] (thin curves). Amplitude modulation function of the order parameter $a(r) = |\Psi(r)|/|\Psi(\infty)|$ for a vortex at different temperatures and scattering lengths. The results of the present theory (heavy curves) are compared with the BdG data of reference [42] (thin curves).

The superfluid density determined by (33) explicitly leads to the expression

$$\rho_{sf} = \frac{|\Psi|^2}{3m^2}\int \frac{d\mathbf{k}}{(2\pi)^3}k^2\; f_2\left(\beta, E_{\mathbf{k}}, \zeta\right). \tag{35}$$

Remarkably, this expression corresponds exactly to the Landau-type formula for a Fermi superfluid, but now extended throughout the whole BCS-BEC crossover, similarly to reference [43]. The total superfluid density, as shown in reference [43], consists of two parts: the mean-field contribution, that is equivalent to (35), and a fluctuation contribution. The fluctuation contribution was also considered in the microscopic rederivations of the Berezinskii-Kosterlitz-Thouless theory based on a path-integral treatment of phase fluctuations in two-dimensional Fermi gases within the low-wavelength

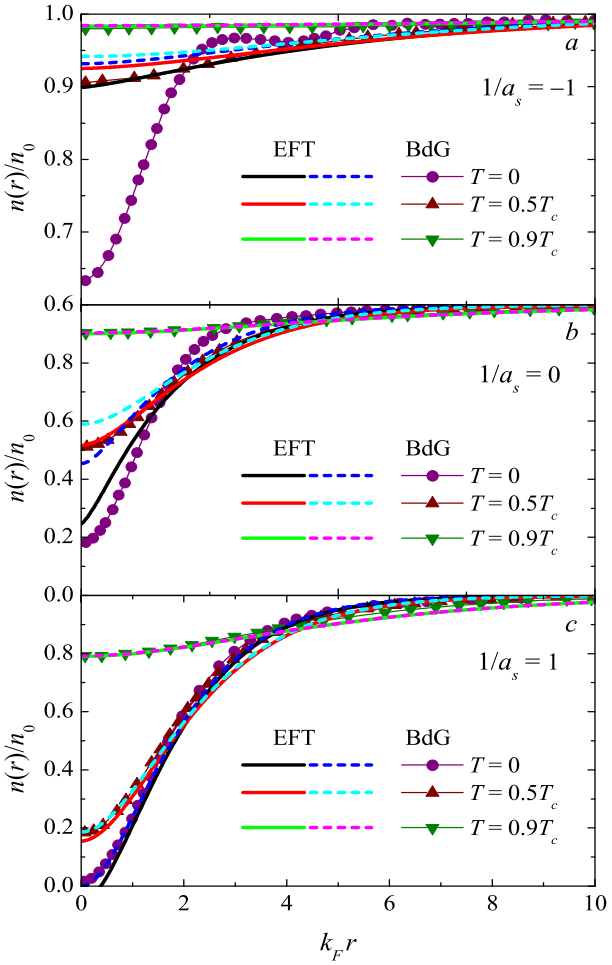

Fig. 3. Density distribution (in units of the bulk density n_0) for a vortex at different temperatures and scattering lengths. The results of the present theory (curves) are compared with the BdG data of reference [42] (symbols). The density calculated within LDA is shown by the solid curves, and the density calculated accounting for the gradient terms is shown by the dashed curves.

approximation [32,33,44]. The superfluid density entering the phase action as a prefactor at $(\nabla\theta)^2$ in these works can be obtained from (35) by a straightforward translation of the present formalism to the two-dimensional case. These two examples represent a reassuring analytic verification of the present formalism as they agree with well-established preceding results.

As was also the case for the order parameter, the agreement between BdG and EFT is gradually better for higher temperatures and/or when moving to the BEC side, where EFT retrieves the Gross-Pitaevskii theory. The gradient corrections improve the agreement between BdG and EFT in the BCS and unitarity regimes. However, in the BEC regime the gradient corrections are extremely small, except at $T = 0$. In the low-temperature limit, the gradient corrections in the BEC regime result in a small artifact: the density goes to negative values near the vortex center. Thus in the BEC regime, LDA seems to describe the density better than the calculation including the gradient corrections. These results are in agreement with the recent work of reference [45] (citing our approach in Ref. [16] of that paper) where a long-wavelength approximation has been developed for the BdG equations. That approach differs from the present formalism in that we perform the long-wavelength expansion for the exact effective bosonic action rather than for the BdG equations (which are already an approximation). Nevertheless, the results of these two approaches are close to each other.

2.4 Collective excitations

The spectrum of the collective excitations is determined in the following way, similarly to reference [46]. First, we assume that the pair field Ψ is a sum of the uniform and time-independent mean-field value Δ and the fluctuation field φ:

$$\Psi(\mathbf{r},\tau) = \Delta + \varphi(\mathbf{r},\tau), \quad \bar{\Psi}(\mathbf{r},\tau) = \Delta + \bar{\varphi}(\mathbf{r},\tau) \tag{36}$$

and keep the fluctuations up to second order. Next, the pair field is rewritten in the $(q, i\Omega_n)$ representation. This gives us the quadratic fluctuation action in matrix form:

$$S_{EFT}^{(quad)} = \frac{1}{2}\sum_{\mathbf{q},n}(\bar{\varphi}_{\mathbf{q},n}\varphi_{-\mathbf{q},-n}) \times \mathbb{M}(q, i\Omega_n)\begin{pmatrix}\varphi_{\mathbf{q},n}\\ \bar{\varphi}_{-\mathbf{q},-n}\end{pmatrix}, \tag{37}$$

where the matrix $\mathbb{M}(q, i\Omega_n)$ is determined by:

$$\begin{aligned} M_{1,1}(q, i\Omega_n) &= \mathcal{U} + \frac{\mathcal{C}}{2m}q^2 - i\Omega_n\tilde{\mathcal{D}} + \Omega_n^2\mathcal{Q},\\ M_{1,2}(q, i\Omega_n) &= \mathcal{U} - \frac{\mathcal{E}}{m}q^2 - \mathcal{R}\Omega_n^2,\\ M_{2,1}(q, i\Omega_n) &= M_{1,2}(q, -i\Omega_n),\\ M_{2,2}(q, i\Omega_n) &= M_{1,1}(q, -i\Omega_n), \end{aligned} \tag{38}$$

with the coefficients introduced in (14)–(21) and

$$\mathcal{U}(w) = w\frac{\partial^2\Omega_s(w)}{\partial w^2}, \quad \tilde{\mathcal{D}}(w) = \frac{\partial[w\mathcal{D}(w)]}{\partial w}, \tag{39}$$

$$\mathcal{C} = \tilde{\mathcal{C}} - 2\mathcal{E}, \quad \mathcal{Q} = \tilde{\mathcal{Q}} - \mathcal{R}. \tag{40}$$

The spectra of collective excitations are determined after the transition $i\Omega_n \to \omega$ as the roots of the equation

$$\det\mathbb{M}(q,\omega) = 0. \tag{41}$$

The solution of equation (41) in the long-wavelength approximation yields the Bogoliubov-Anderson (Goldstone) mode with the frequency

$$\omega_q = v_s q, \tag{42}$$

where v_s is the first sound velocity. It is expressed through the coefficients of the effective field action similarly to references [46,47]:

$$v_s = \sqrt{\frac{1}{m}\frac{\mathcal{U}\tilde{\mathcal{C}}}{\tilde{\mathcal{D}}^2 + 2\mathcal{U}\tilde{\mathcal{Q}}}}. \tag{43}$$

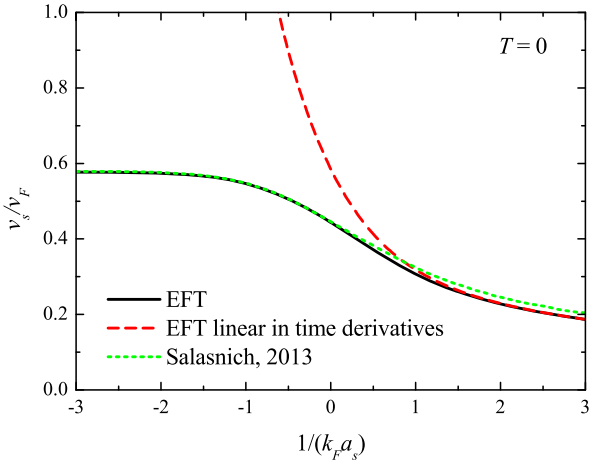

Fig. 4. The sound velocity v_s calculated using formula (43) (solid curve) and neglecting the second time derivative (dashed curve), compared with the result of reference [48] for a 3D Fermi gas.

Note that the coefficient $\tilde{\mathcal{Q}}$ corresponding to the second order of the derivative expansion for the time derivatives enters the sound velocity together with the first order coefficient $\tilde{\mathcal{D}}$. This result demonstrates that the second order of the derivative expansion is important for the spectrum of collective excitations.

In the zero temperature limit, the coefficients entering the matrix (38) for the quadratic fluctuation action correspond exactly to those obtained within the Gaussian pair fluctuation (GPF) theory [46] and in the zero-temperature theory of reference [29]. Remarkably, despite the fact that the approach of reference [29] is non-perturbative (i.e. without assuming the non-uniform part of the pair field to be small), the coefficients for the zero-temperature action functional in reference [29] appear to be the same as in the GPF at $T = 0$ [46]. In other words, at zero temperature, the result of two approximations (small fluctuations and slowly varying fluctuations) does not depend on their sequence. On the contrary, at nonzero temperatures these two approximations do not commute.

In Figure 4, the sound velocity v_s (in units of the Fermi velocity $v_F \equiv \hbar k_F/m$) calculated using the mean-field values of the chemical potential is plotted as a function of the inverse scattering length and compared with that extracted from reference [48] for a Fermi gas in three dimensions. In that paper, the effect of both phase and amplitude fluctuations of the order parameter is taken into account in the determination of the sound velocity of the uniform superfluid system in the BCS-BEC crossover. The results obtained in reference [48] depend strongly on whether amplitude fluctuations are taken into account or not. The amplitude fluctuations are incorporated in reference [48] following Schakel [30], obtaining results at the unitarity regime and at $T = 0$. The present calculation also takes into account both phase and amplitude fluctuations, at all coupling strengths and temperatures. We can see from Figure 4 that our result for v_s and that of reference [48] agree excellently at the BCS side, and exhibit only a slight difference in the BEC regime.

In order to show the importance of the terms of second order in the time derivative, we show in Figure 4 also the sound velocity determined within our EFT neglecting the coefficient $\tilde{\mathcal{Q}}$ in (43). It is clear that setting $\tilde{\mathcal{Q}} = 0$ leads to a substantial change in the BCS regime, while leaving the result in the BEC regime unaffected.

3 Two-band Fermi superfluids

3.1 Extension of the EFT to two bands

The extension of the EFT formulated in the above subsection to the two-band Fermi systems is particularly interesting due to recent intense discussions on the applicability of the GL approach to the coupled Fermi systems far below T_c [17–23].

Here, we consider a fermionic system of two types of particles ($j = 1, 2$) with two spin states each described by the microscopic atomic Hamiltonians $H_{\sigma,j}$ as in the section on the one-band system, with possibly different masses and chemical potentials for each band. The path-integral scheme remains the same as above. The interaction Hamiltonian $U(\mathbf{r}, \tau)$, however, is more complicated, because it describes both intraband and interband interactions:

$$\begin{aligned} U = & \sum_{j=1,2} g_j \bar{\psi}_{\uparrow,j} \bar{\psi}_{\downarrow,j} \psi_{\downarrow,j} \psi_{\uparrow,j} \\ & + g_3 \left(\bar{\psi}_{\uparrow,1} \psi_{\uparrow,1} \bar{\psi}_{\downarrow,2} \psi_{\downarrow,2} + \bar{\psi}_{\downarrow,1} \psi_{\downarrow,1} \bar{\psi}_{\uparrow,2} \psi_{\uparrow,2} \right) \\ & + g_4 \left(\bar{\psi}_{\uparrow,1} \psi_{\uparrow,1} \bar{\psi}_{\uparrow,2} \psi_{\uparrow,2} + \bar{\psi}_{\downarrow,1} \psi_{\downarrow,1} \bar{\psi}_{\downarrow,2} \psi_{\downarrow,2} \right) . \end{aligned} \quad (44)$$

The terms with the coupling constants g_1, g_2 determine the intraband scattering between two fermions of the same type and with antiparallel spins: these are the two Cooper pairing channels. The terms with g_3 and g_4 are related to the interband scattering for the fermions with antiparallel and parallel spins, respectively. In ultracold gases, scattering between fermions with parallel spins is not present for fermions in the same band due to the Pauli principle. However, parallel spin scattering between fermions in *different* bands should be kept, as it contributes to the renormalization of the effective interaction. Terms of the type $\bar{\psi}_{\downarrow,1} \bar{\psi}_{\uparrow,1} \psi_{\downarrow,2} \psi_{\uparrow,2}$ are not included in the interaction Hamiltonian (44). They are kept in some theoretical schemes (e.g. [8,9,13]) and describe an ad hoc model interband scattering of pairs. However, we avoid such terms in the starting microscopic action because they cannot arise from any density-density type of interaction.

The Hubbard-Stratonovich (HS) transformation is based on introducing auxiliary fields Ψ_j and χ_j such that the relation

$$\mathcal{Z} \propto \int \mathcal{D}\left[\bar{\psi}, \psi\right] \int \mathcal{D}\left[\bar{\Psi}, \Psi\right] \int \mathcal{D}\left[\bar{\chi}, \chi\right] e^{-S_{HS}} \quad (45)$$

is satisfied. In the HS action S_{HS}, the fermion fields appear only up to quadratic order so they can be integrated.

The HS action which exactly decouples the four-field interaction terms in the initial Hamiltonian, involves two pair fields and two density fields corresponding to the interband normal channel (see Ref. [49]):

$$S_{HS} = S_0 + S_B + S_\chi + \sum_{j=1,2} \int_0^\beta d\tau \int d\mathbf{r} \Big(\bar{\Psi}_j \psi_{j,\uparrow} \psi_{j,\downarrow} + \Psi_j \bar{\psi}_{j,\downarrow} \bar{\psi}_{j,\uparrow} + i\bar{\chi}_j \rho_j + i\chi_j \bar{\rho}_j \Big), \tag{46}$$

where $\rho_1 = \bar{\psi}_{1,\uparrow}\psi_{2,\downarrow} + \bar{\psi}_{2,\uparrow}\psi_{1,\downarrow}$ and $\rho_2 = \bar{\psi}_{1,\uparrow}\psi_{2,\uparrow} + \bar{\psi}_{2,\downarrow}\psi_{1,\downarrow}$ are combinations of the fermion variables, Ψ_j and χ_j are the HS pair and density fields, respectively. The actions of the free HS fields are given by:

$$S_B = -\int_0^\beta d\tau \int d\mathbf{r} \left[\frac{1}{G_1} \bar{\Psi}_1 \Psi_1 + \frac{1}{G_2} \bar{\Psi}_2 \Psi_2 - \frac{1}{G_{12}} \left(\bar{\Psi}_1 \Psi_2 + \bar{\Psi}_2 \Psi_1 \right) \right], \tag{47}$$

$$S_\chi = -\int_0^\beta d\tau \int d\mathbf{r} \left(\frac{1}{g_3} \bar{\chi}_1 \chi_1 + \frac{1}{g_4} \bar{\chi}_2 \chi_2 \right). \tag{48}$$

The intraband channel for same-spin fermions is not present (nor is it in Ref. [11]) because we assume the temperature is low enough so that only s-wave scattering occurs. The four-field HS transformation exactly eliminates the fermion-fermion interaction from the initial Hamiltonian. If the interband coupling is switched off, the effective bosonic action exactly turns to that exploited in reference [11] for two independent bands.

Although there is no Josephson interband coupling in the initial fermion-fermion interaction (44), this coupling emerges in a natural way in the effective bosonic action (47) and follows explicitly from the HS transformation of the microscopic action. The coupling constants G_j are related to those from (44) in the following way:

$$\frac{1}{G_1} = \frac{g_2}{g_1 g_2 - g_{12}^2}, \quad \frac{1}{G_2} = \frac{g_1}{g_1 g_2 - g_{12}^2}, \quad \frac{1}{G_{12}} = \frac{g_{12}}{g_1 g_2 - g_{12}^2}, \quad g_{12} = g_4 - g_3. \tag{49}$$

In order to address the whole range of the BCS-BEC crossover, the coupling constants g_1, g_2 are renormalized through the s-wave scattering lengths $a_{s,j}$ similarly to reference [11] and in the above subsection for the one-band system:

$$\frac{1}{g_j} = m_j \left(\frac{1}{4\pi a_{s,j}} - \int_{k<K} \frac{d\mathbf{k}}{(2\pi)^3} \frac{1}{k^2} \right) \tag{50}$$

with $K \to \infty$. In order to ensure convergence in the thermodynamic potential and in the gap equation, the other two coupling constants g_3, g_4 must also be renormalized through equation (50), with the scattering lengths $a_{s,3}$ and $a_{s,4}$ and the mass parameter $m_3 = m_4 \equiv m_{12}$. The mass parameter m_{12}, as shown below, enters the final results through the factor γm_{12} with the interband coupling parameter $\gamma \equiv 2(\frac{1}{a_{s,3}} - \frac{1}{a_{s,4}})$. Consequently this mass can be chosen arbitrary as far as the renormalization is concerned, and we set $m_{12} = \sqrt{m_1 m_2}$. With these renormalizations, $g_{12}^2/(g_1 g_2) \propto 1/K^2$, so that the stability condition $g_1 g_2 > g_{12}^2$ is always fulfilled.

The integration over the fermion fields leads to the partition function,

$$\mathcal{Z} \propto \int \mathcal{D}\left[\bar{\Psi}, \Psi\right] \int \mathcal{D}\left[\bar{\chi}, \chi\right] e^{-S_{\text{eff}}}, \tag{51}$$

with the effective bosonic action S_{eff}. The details for the effective bosonic action are described in the Appendix. The ultraviolet-divergent part of the effective bosonic action can be explicitly extracted. When introducing a sufficiently large momentum cutoff k_0 for the fermion fields, the part of the HS action for $k > k_0$ provides the ultraviolet-divergent part of the effective bosonic action

$$\delta S_{\text{eff}}^{(\text{div})}(k_0) = -\int_0^\beta d\tau \int d\mathbf{r} \int_{(k>k_0)} \frac{d\mathbf{k}}{(2\pi)^3} \sum_{j=1,2} \frac{m_j}{k^2} \times \bar{\Psi}_j(\mathbf{r},\tau) \Psi_j(\mathbf{r},\tau) + O\left(k^{-4}\right). \tag{52}$$

The density fields χ_j do not contribute to the ultraviolet divergence of the effective bosonic action. In the limit $|g_j| \to \infty$ (corresponding to $K \to \infty$), the divergence of the action S_B is exactly compensated by (52) using (50), so that the part of the effective action depending on the pair fields Ψ_j is regularized. On the contrary, the density-field action S_χ unrestrictedly increases when $K \to \infty$. Thus the functional e^{-S_χ} acts as a product of delta functions for the density fields $\chi_j(\mathbf{r},\tau)$ at all $(\mathbf{r},\tau)$. As a result, the subsequent integration over the density fields is performed exactly, and we arrive at the effective bosonic action depending on the pair fields only:

$$S_{\text{eff}} = S_B - \sum_{j=1,2} \text{Tr} \ln \left[-\mathbb{G}_j^{-1} \right]. \tag{53}$$

The inverse Nambu tensor $\mathbb{G}_j^{-1}$ for each band has been determined above. In the effective field action (53), the coupling strengths of the starting Hamiltonian are reduced to only three input parameter of the theory: two scattering lengths $a_{s,1}, a_{s,2}$ and the Josephson interband coupling strength γ. The intraband coupling strengths (expressed here through the scattering lengths) and the interband coupling strength are the standard input parameter which are used in known works of two-band superconductivity/superfluidity (see, e.g. Refs. [1,8–10,13]). These parameters are measurable: the scattering lengths and the Josephson interband coupling strength can be experimentally determined and controlled using e.g. the Feshbach resonance.

The effective action (53) is expanded as a series in powers of the pair field in the same way as for a one-band system. Correspondingly, the derivative expansion and the summation over the whole series in powers of the

pair fields is performed for each band independently. As a result, the bosonic action $S_{\rm eff}$ is approximated by the following effective field action $S^{(2b)}_{EFT}$:

$$S^{(2b)}_{EFT} = \sum_{j=1,2} S^{(j)}_{EFT} - \int_0^\beta d\tau \int d\mathbf{r}\, \frac{m_{12}\gamma}{4\pi} \left(\bar{\Psi}_1\Psi_2 + \bar{\Psi}_2\Psi_1\right), \tag{54}$$

where $S^{(j)}_{EFT}$ is the effective field action for each band determined by (16).

The equations of motion for the order parameters follow from the stationary action principle, resulting in a set of four coupled equations. Two equations – for $j = 1$ and $j = 2$ – are:

$$\begin{aligned} i\frac{\partial\left(w_j\mathcal{D}_j\right)}{\partial w_j}\frac{\partial\Psi_j}{\partial t} &= \mathcal{A}_j\left(w_j\right)\Psi_j - \frac{m_{12}\gamma}{4\pi}\Psi_{3-j} \\ &+ \mathcal{Q}_j\frac{\partial^2\Psi_j}{\partial t^2} - \frac{\mathcal{R}_j\Psi_j^2}{w_j}\frac{\partial^2\bar{\Psi}_j}{\partial t^2} \\ &- \frac{1}{w_j}\frac{\partial\left(w_j\mathcal{R}_j\right)}{\partial w_j}\Psi_j\frac{\partial\bar{\Psi}_j}{\partial t}\frac{\partial\Psi_j}{\partial t} \\ &+ \left(\frac{\partial\mathcal{Q}_j}{\partial w_j} + \frac{1}{2w_j}\frac{\partial\left(w_j\mathcal{R}_j\right)}{\partial w_j}\right)\bar{\Psi}_j\left(\frac{\partial\Psi_j}{\partial t}\right)^2 \\ &- \frac{1}{2}\frac{\partial\left(\frac{\mathcal{R}_j}{w_j}\right)}{\partial w_j}\Psi_j^3\left(\frac{\partial\bar{\Psi}_j}{\partial t}\right)^2 \\ &- \frac{\mathcal{C}_j}{2m_j}\nabla^2_{\mathbf{r}}\Psi_j + \frac{\mathcal{E}_j\Psi_j^2}{m_jw_j}\nabla^2_{\mathbf{r}}\bar{\Psi}_j \\ &+ \frac{1}{m_jw_j}\frac{\partial\left(w_j\mathcal{E}_j\right)}{\partial w_j}\Psi_j\left(\nabla_{\mathbf{r}}\bar{\Psi}_j\cdot\nabla_{\mathbf{r}}\Psi_j\right) \\ &- \frac{1}{2m_j}\left(\frac{\partial\mathcal{C}_j}{\partial w_j} + \frac{1}{w_j}\frac{\partial\left(w_j\mathcal{E}_j\right)}{\partial w_j}\right) \\ &\times\bar{\Psi}_j\left(\nabla_{\mathbf{r}}\Psi_j\right)^2 + \frac{1}{2m_j}\frac{\partial\left(\frac{\mathcal{E}_j}{w_j}\right)}{\partial w_j}\Psi_j^3\left(\nabla_{\mathbf{r}}\bar{\Psi}_j\right)^2, \end{aligned} \tag{55}$$

and the other two equations are conjugate to (55). Within the local-density approximation (LDA) time and space derivatives in (55) are neglected and we obtain two coupled gap equations,

$$\mathcal{A}_j\left(w_j\right)\Psi_j - \frac{m_{12}\gamma}{4\pi}\Psi_{3-j} = 0. \tag{56}$$

The two-band effective action allows for mass imbalance $m_1 \neq m_2$. This can be important for two-band superconductors but seems to be less relevant for ultracold atomic gases, because phase coherence and Josephson coupling between species with different masses are hardly achievable. In the treatment of applications of the EFT in the present paper, we assume no mass imbalance. Consequently, for the numerical calculations we use the same set of units as in Section 2.

3.2 Uniform two-band superfluid

3.2.1 Parameters and thermodynamic functions at $T = 0$

In two-bandgap Fermi superfluids, the interband interactions compete with the intraband interactions and affect the ground-state phases. The thermodynamic potential per unit volume for the uniform two-band system resulting from the action functional (54) is:

$$\Omega = \sum_{j=1,2}\Omega_{s,j} - \frac{m_{12}\gamma}{4\pi}\left(\bar{\Psi}_1\Psi_2 + \bar{\Psi}_2\Psi_1\right). \tag{57}$$

At zero temperature, the mean-field thermodynamic potential adequately describes the properties of the Fermi superfluid in the whole range of the BCS-BEC crossover. The internal energy as a function of the total fermion particle density n, is determined at $T = 0$ through the thermodynamic relation

$$E = \Omega + \mu n. \tag{58}$$

In the present treatment we assume that the masses of the fermions in the two subbands are the same, the band offset is equal to zero, and the subbands are in thermodynamical equilibrium in the sense that their chemical potentials are equal. The number equation

$$-\frac{\partial\Omega}{\partial\mu} = n \tag{59}$$

determines the chemical potential that is common for both bands. The three parameters Ψ_1, Ψ_2, μ are found by solving the number equation (59) along with the two coupled gap equations (56). The roots of this coupled set of equations are derived numerically, and we investigate the dependence of these solutions on the interband coupling γ and on the intraband coupling parameters $1/a_{s,j}$ where $a_{s,j}$ is the scattering length between fermions in band j.

In Figure 5a, the order parameters for a two-band superfluid Fermi gas are plotted as a function of the interband coupling strength γ for the inverse scattering length of the "stronger" band $1/a_{s,1} = 0$ and for different values of the inverse scattering length of the "weaker" band $1/a_{s,2}$. As intuitively expected, both Ψ_1 and Ψ_2 are monotonously increasing functions of the interband coupling strength γ. The difference $\Psi_2 - \Psi_1$ is an increasing function of the difference $1/a_{s,1} - 1/a_{s,2}$.

Figure 5 reveals some surprising details of the interplay between the interband and intraband couplings. At large γ, the dependence of Ψ_1 on $1/a_{s,2}$ has the same sign as that of Ψ_2 on $1/a_{s,2}$. However, at small γ (here, $\gamma \lessapprox 0.35$), the order parameter Ψ_1 becomes a decreasing function of $1/a_{s,2}$ and this behavior persists even at zero coupling where one expects Ψ_1 to be independent of $a_{s,2}$. This behavior of the order parameter can be explained by a population transfer between bands. Indeed, even in the limit of the zero coupling, the common chemical potential leads to unequal fermion densities in the two bands, and in particular, to a depletion of the weak band. The common chemical potential will be affected by the scattering

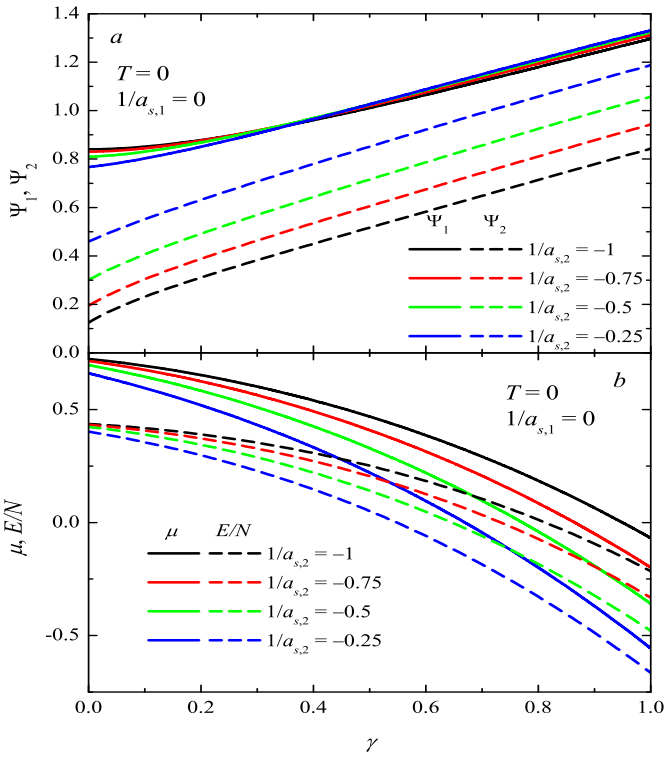

Fig. 5. (a) Order parameters Ψ_1 (solid curves) and Ψ_2 (dashed curves); (b) chemical potential (solid curves) and internal energy (dashed curves) for a two-band superfluid Fermi gas as a function of the interband coupling strength γ for the inverse scattering length of the "stronger" band $1/a_1 = 0$ and for different values of $1/a_2$.

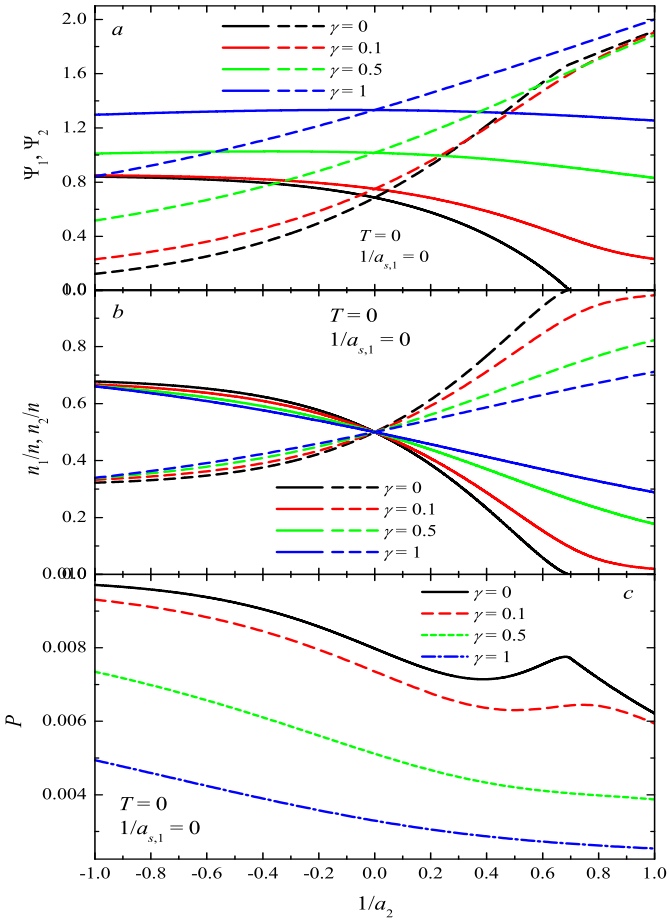

Fig. 6. (a) Order parameters Ψ_1 (solid curves) and Ψ_2 (dashed curves); (b) fermion densities in the first band (solid curves) and second band (dashed curves); (c) pressure for a two-band superfluid Fermi gas as a function of the inverse scattering length $1/a_{s,2}$, for $1/a_{s,1} = 0$ and for different values of the interband coupling strength γ.

lengths of both bands, even in the limit of zero interaction coupling between different bands, and this results in a population transfer between the bands. The "stronger" band drains away more fermions from the "weaker" band as the difference between the inverse scattering lengths $1/a_{s,1} - 1/a_{s,2}$ grows. These additional fermions allow to form more pairs, resulting in an increase of Ψ_1 as $1/a_{s,2}$ becomes more negative.

In Figure 5b, we show the common chemical potential μ and the internal energy per particle E/n as a function of the interband coupling strength γ, for several values of the inverse scattering $1/a_{s,2}$ length of the "weaker" band. We can see that an increasing *inter*band coupling acts like an increasing *intra*band coupling: both the chemical potential and the internal energy decrease when γ rises. In the BEC limit, the difference between E/n and μ gradually decreases, while at all coupling $E/n < \mu$. This inequality must necessarily be fulfilled, because the thermodynamic potential per unit volume is equal to minus the pressure: $\Omega = -P$ and the pressure remains positive.

In Figure 6a we return to the question of population transfer between the bands, and plot the order parameters as a function of $1/a_{s,2}$, for $1/a_{s,1} = 0$ and for several values of γ. Here, the interaction parameter of the second band crosses over from the BCS regime at $1/a_{s,2} = -1$ to the BEC regime at $1/a_{s,2} = 1$. In the range $1/a_{s,2} < 0$, the first band is the "stronger" band, and for $1/a_{s,2} > 0$, the first band is the "weaker" band. In the BEC regime, we find a remarkable feature: Ψ_1 can turn to zero when $1/a_{s,2}$ is sufficiently large and γ is sufficiently small (here, at $\gamma = 0$). At this critical point, also Ψ_2 reveals a kink.

The origin of this suppression of Ψ_1 becomes clear when we look at the dependence of the relative fermion densities for the first and second band as a function of $1/a_{s,2}$, shown in Figure 6b. We again see that, even when $\gamma = 0$, the common chemical potential couples the bands through population transfer. As γ grows, this population transfer is reduced. In the BEC range, the population transfer is more pronounced, and when γ is small and $1/a_{s,2}$ is sufficiently large, the population transfer can completely deplete the first band, driving Ψ_1 down to zero. This possibility has gone hitherto unnoticed in the theoretical descriptions of two-band systems, as these are usually studied in the BCS limit. Even in strong-coupling superconductors, the BEC regime seems not to be achieved. Therefore this effect seems to be a new feature related to the Fermi gases

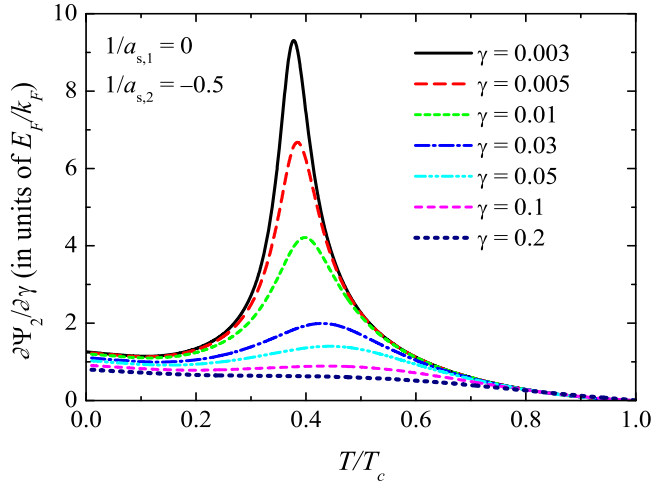

Fig. 7. Susceptibility $\partial\Psi_2/\partial\gamma$ for the "weaker" band as a function of T/T_c for inverse scattering lengths $1/(k_F a_{s,1}) = 0$ and $1/(k_F a_{s,2}) = -0.5$. Here, T_c is the critical temperature for the two-band system.

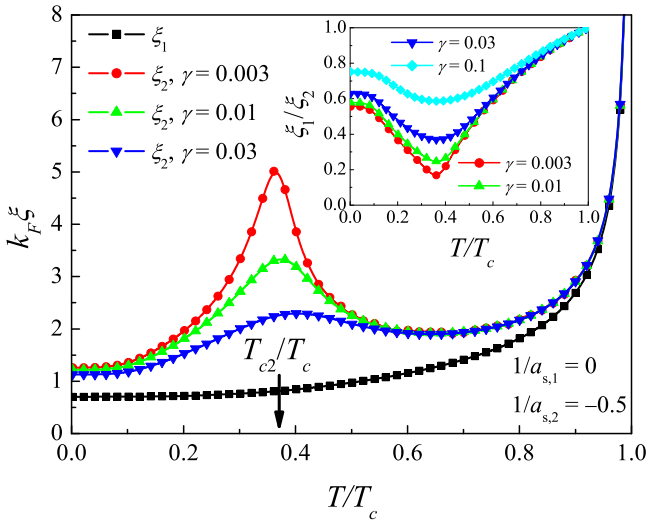

Fig. 8. The healing lengths ξ_j corresponding to the stronger ($j = 1$) and weaker ($j = 2$) bands are shown as a function of temperature for different coupling parameters γ. The inset shows the ratio ξ_1/ξ_2.

where the BCS-BEC crossover regime can be experimentally probed.

The effect of band population transfer can also been seen in the dependence of the pressure $P = -\Omega$ on $1/a_{s,2}$, shown in Figure 6c. The pressure exhibits a local maximum for the curve with $\gamma = 0$ when the "weaker" band becomes completely depleted. Moreover, when γ is nonzero but sufficiently small, the pressure depends on $1/a_{s,2}$ non-monotonically.

3.2.2 Temperature dependence of parameters

As shown in reference [23], a Josephson coupling for two-bandgap superconductors yields the symmetry breakdown from $U(1) \times U(1)$ to $U(1)$ and hence eliminates the superconducting phase transition for a "weaker" band at $T_{c,2}$, where $T_{c,2}$ is the critical temperature for the "weaker" band in the absence of interband coupling. As a result, the divergence of the coherence length is removed for the "weaker" band. For a sufficiently small interband coupling, one of the coherence lengths has a peak near $T_{c,2}$. This peaked behavior of the coherence length and related quantities was also considered in reference [50], where it was referred to as "hidden criticality". The peaked behavior near $T_{c,2}$ is most clearly revealed in the γ susceptibility of the order parameters, $\partial\Psi_j/\partial\gamma$. There is no true criticality in a two-band fermion system at $T < T_c$. Rather, the terminology introduced in reference [50] emphasizes the fact that the coupled system is still affected by the proximity of the weaker band.

We find that the non-monotonic temperature dependence of the thermodynamic quantities is also present in two-bandgap superfluid atomic Fermi gases, as shown in Figure 7. For sufficiently weak interband coupling, a peak appears in $\partial\Psi_2/\partial\gamma$ at $T \approx T_{c,2}$. Note that in the standard GL model a non-physical divergence of $\partial\Psi_2/\partial\gamma$ occurs at $T_{c,2}$: in order to find a finite susceptibility peak the Bogoliubov-de Gennes (BdG) equations had to be used in reference [50]. We find that our present formalism, like the BdG equations, leads to a convergent susceptibility at $T \approx T_{c,2}$.

As already indicated above, a common chemical potential for the two bands can lead to a partial depletion of the population of the "weak" band. This will also affect the critical temperature $T_{c,2}$ corresponding to the weak band, even at zero interband coupling, $\gamma = 0$. This effect, to the best of our knowledge, did not attract attention in past works on multiband superconductors, as these consider only the BCS limit for the scattering lengths, where the feedback of the gap parameter to the density and to the number equations is negligible.

Having obtained the bulk values Ψ_1 and Ψ_2 for a uniform (bulk) system, the healing lengths can be determined for the two-bandgap case by substituting $\Psi_j(r) = \Psi_j^{(bulk)} \tanh(x/\sqrt{2}\xi_j)$ in the EFT energy functional for a stationary pair field. This variational "trial function" describes how a two-bandgap superfluid in a semi-infinite space heals from a wall at $x = 0$ back to the bulk values $\Psi_j^{(bulk)}$ of the band gaps. The healing lengths ξ_j are determined variationally and the result is shown in Figure 8. We find, in agreement with reference [17], that the ratio of healing lengths converges to 1 in the limit $T \to T_c$. The obtained peaked behavior of the healing length ξ_2 near $T_{c,2}$ also agrees with the results of references [23,50] derived using a very different method. These healing lengths will also determine the structure of vortices in the fermionic superfluids. In superconductors, the London penetration depth comes into play as a second length scale, but the experiments on quantum gases work with neutral atoms so that there is no coupling to the vector potential.

The healing length calculated here from the vortex profiles should be distinguished from the pair correlation

length as discussed in reference [51]. The latter should be calculated from the correlation function $g_{\uparrow\downarrow}(\rho)$ as in reference [51].

3.3 Spectra of collective modes

In a two-band system, the Bogoliubov-Anderson (Goldstone) collective mode should also exist, as in a one-band system. The existence of a Goldstone mode is a universal result, caused by the spontaneous breakdown of gauge symmetry associated with the superfluid phase transition. In addition, another collective mode can appear in a two-band system, as first derived by Leggett [52] for a two-band BCS superconductor. The Leggett mode has been observed in MgB_2 using Raman scattering [53], but to the best of our knowledge, it has not yet been observed in multi-component atomic Fermi gases. This has not stopped theoretical efforts to consider two-band Fermi superfluids in the BCS-BEC crossover regime at zero temperature [8,9]. In references [8,9] the model interband Josephson interaction is present already in the starting Hamiltonian, and the interaction is measured in terms of potentials rather than scattering lengths. In the present treatment, the Josephson interaction emerges from the interatomic scattering interactions. Nevertheless, we can perform a qualitative comparison of our results with those of references [8,9].

The spectrum of collective excitations in a one-band system was determined solving the equation (41) where the dynamic matrix $\mathbb{M}(q,\omega)$ is given by (38). As follows from the effective action (37), the dynamic matrix for the two-band system is a 4×4 matrix that can be written as

$$\mathbb{M}^{(2band)}(q,\omega)=\begin{pmatrix}\mathbb{M}_1(q,\omega)+\varkappa\eta\cdot\mathbb{I} & -\varkappa\mathbb{I}\\ -\varkappa\mathbb{I} & \mathbb{M}_2(q,\omega)+\frac{\varkappa}{\eta}\cdot\mathbb{I}\end{pmatrix}, \tag{60}$$

where $\mathbb{M}_j(q,\omega)$ are the dynamic matrices for each band, $\mathbb{I}$ is the unit 2×2 matrix, $\varkappa$ is proportional to the interband coupling strength $\varkappa\equiv\frac{m_{12}\gamma}{4\pi}$, and $\eta=\frac{|\Psi_2|}{|\Psi_1|}$ is the ratio of the gap parameters for two bands. The eigenfrequencies of the collective excitations are determined by the roots of the equation

$$\det\mathbb{M}^{(2band)}(q,\omega)=0. \tag{61}$$

We are searching for the eigenfrequencies at small momenta q, that is in accordance with the approximation of slowly varying pair fields. Therefore the roots of the equation (61) are approximated by the leading terms of the Taylor series in powers of the momentum, similarly as for the one band system.

Bogoliubov-Anderson mode

The Bogoliubov-Anderson mode at small q is an acoustic mode $\omega_q=v_s q$ determined by the sound velocity v_s. For the two-band system we find:

$$v_s=\left\{\left(\varkappa\left(\mathcal{U}_1+\eta^2\mathcal{U}_2\right)+2\eta\mathcal{U}_1\mathcal{U}_2\right)\left(\frac{\tilde{\mathcal{C}}_1}{m_1}+\eta^2\frac{\tilde{\mathcal{C}}_2}{m_2}\right)\right.$$
$$\times\left[\varkappa\left(\tilde{\mathcal{D}}_1+\eta^2\tilde{\mathcal{D}}_2\right)^2+2\eta\left(\tilde{\mathcal{D}}_1^2\mathcal{U}_2+\eta^2\tilde{\mathcal{D}}_2^2\mathcal{U}_1\right)\right.$$
$$\left.\left.+2\left(\varkappa\mathcal{U}_1+\varkappa\eta^2\mathcal{U}_2+2\eta\mathcal{U}_1\mathcal{U}_2\right)\left(\tilde{\mathcal{Q}}_1+\eta^2\tilde{\mathcal{Q}}_2\right)\right]^{-1}\right\}^{1/2}. \tag{62}$$

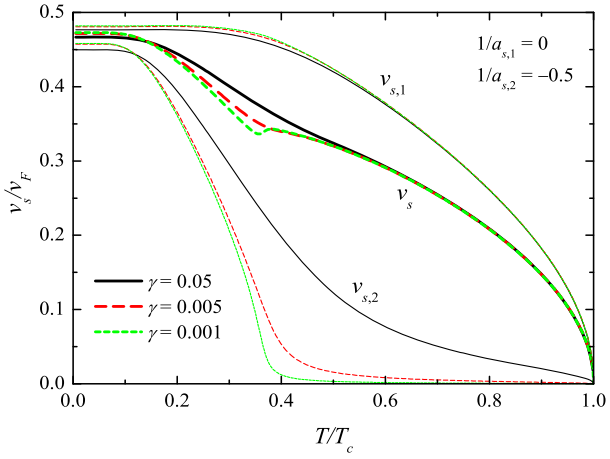

Fig. 9. *Heavy curves*: the sound velocity in a two-band superfluid Fermi gas as a function of the temperature for $1/a_{s,1}=0$, $1/a_{s,2}=-0.5$, with different values of the interband coupling parameter γ. *Thin curves*: the one-band sound velocity parameters $v_{s,1}$ and $v_{s,2}$ described in the text.

In Figure 9, the temperature dependence of the sound velocity in a two-band system is shown. We plot the sound velocity as a function of temperature for $1/a_{s,1}=0$ and $1/a_{s,2}=-0.5$, using different values of the interband coupling parameter γ. For comparison, the one-band sound velocities for each band are shown in the same graph by thin curves. They are calculated using formula (43) with the parameters $(\beta,\mu,|\Psi|)$ attributed to each band in the *coupled* two-band system (rather than with the parameters for an independent one-band system). In other words, in the figure, $v_{s,j}=v_s^{(1band)}(\beta,\mu,|\Psi_j|)$, where $|\Psi_j|$ are determined from the coupled gap equations (56) for the two-band system with the number equation (59). Under these conditions, the inequality

$$\min(v_{s,1},v_{s,2})\le v_s\le\max(v_{s,1},v_{s,2})$$

is fulfilled. It should be noted that $v_{s,1},v_{s,2}$ are not the true sound velocities in the two-band system: they are only auxiliary parameters. There is a unique first sound velocity v_s for the whole system given by (62).

We see from Figure 9 that $v_{s,2}$ shows a rapid decrease for temperatures near $T_{c,2}<T_c$. This decrease of $v_{s,2}$ becomes more gradual as the interband coupling γ becomes larger. This is reflected in the behavior of $v_s(T)$: near T_c the sound velocity of the Bogoliubov-Anderson mode shows a dip.

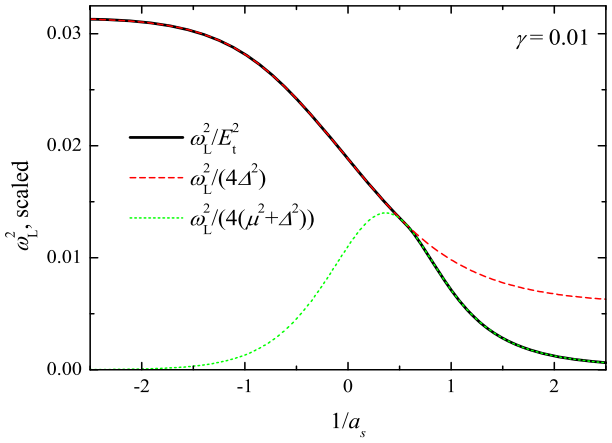

Fig. 10. The frequency (squared) of the Leggett mode for a two-band Fermi gas at $T = 0$ is shown as a function of $1/a_s$ for the interband coupling $\gamma = 0.01$. The Leggett mode frequency is scaled by the two-quasiparticle threshold $E_t \equiv \min(2E_{\mathbf{k}})$ (full line), 2Δ (thin dashed line) and $2\sqrt{\Delta^2+\mu^2}$ (thin dot-dashed line), respectively.

Leggett mode

The Leggett mode is specific for two-band superfluids as it describes small oscillations of the relative phase of two condensates. In the long-wavelength approximation, the frequency of the Leggett mode can be approximately written as:

$$\omega_L(q) \approx \sqrt{\omega_{L,0}^2 + v_L^2 q^2}, \tag{63}$$

so that it remains gapped in the limit $q \to 0$ (for $\gamma \neq 0$). The frequency of the Leggett mode is determined numerically by solving equation (61). In the long-wavelength approximation an analytic approximation for the Leggett mode frequency can be obtained:

$$\omega_{L,0} \approx \left(\frac{2\mathcal{U}_1 \varkappa\eta}{P_1^2 + 2\mathcal{U}_1\tilde{\mathcal{Q}}_1} + \frac{2\mathcal{U}_1 \frac{\varkappa}{\eta}}{P_2^2 + 2\mathcal{U}_2\tilde{\mathcal{Q}}_2} \right)^{1/2}. \tag{64}$$

In Figure 10, we plot the frequency (squared) of the Leggett mode, $\omega_{L,0}^2$, for a two-band Fermi gas at $T = 0$, as a function of the inverse scattering length $1/a_s = 1/a_{s,1} = 1/a_{s,2}$. The Leggett mode frequency is scaled to the two-particle threshold $E_t \equiv \min(2E_{\mathbf{k}})$ similarly as in reference [8] where E_t is deemed to be the physically reasonable maximal value for the frequency of collective oscillations. This scaling factor is equal to 2Δ for $\mu > 0$ and $2\sqrt{\Delta^2+\mu^2}$ for $\mu < 0$, where $\Delta = \max(|\Psi_1|, |\Psi_2|)$.

We can qualitatively compare the behavior of $\omega_{L,0}^2$ obtained in the present treatment with the result shown in Figure 5 of reference [8]. At present, it is not obvious how the parameters used in the theory of references [8,9] can be matched to the scattering lengths used in our approach. There is a difference between the two theories, because the starting atomic Hamiltonian of reference [9] contains a priori scattering between Cooper pairs, which is not invoked in the present formalism. Nevertheless, we can see a clear similarity between the behavior of $\omega_{L,0}^2$ in reference [8] and in the present treatment.

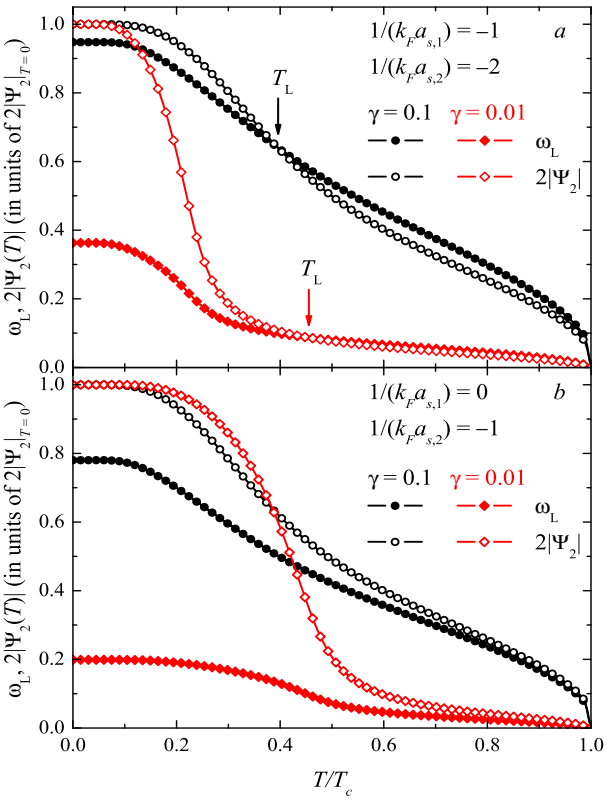

Fig. 11. Temperature dependence of the Leggett mode frequencies ω_L (full symbols) and twice the order parameter $|\Psi_2|$ (hollow symbols) for $1/a_{s,1} = -1$, $1/a_{s,2} = -2$ (a) and for $1/a_{s,1} = 0$, $1/a_{s,2} = -1$ (b), at different values of the interband coupling strength, $\gamma = 0.1$ (circles) and $\gamma = 0.01$ (diamonds).

In Figure 11, the temperature dependence of the Leggett mode frequency is analyzed for different values of the intraband scattering lengths and of the interband coupling strength. The Leggett mode softens with increasing temperature and turns to zero at $T = T_c$. The Leggett mode cannot exist in a one-band system, because it describes oscillations of the relative phase of two condensates. Therefore the Leggett mode frequency must drop down as $T > T_{c,2}$, especially at weak interband coupling. This trend is clearly visible in Figure 11. The behavior of the Leggett mode as a function of temperature obtained in the present formalism agrees qualitatively well with the experimental measurement [54] of this mode in MgB_2, and with different theoretical approaches [55,56].

The observation of the Leggett mode in two-band superconductors was problematic during a long time, because at $\omega_L > 2|\Psi_2|$, the Leggett mode can dissipate to one-particle excitations [52]. Therefore the range of observation for the Leggett mode is approximately restricted by the condition $\omega_L < 2|\Psi_2|$. As pointed out in reference [57], the weak-band order parameter in conventional superconductors is very small, thus making the experimental observation of the Leggett mode rather difficult. However, recently the Leggett mode has been clearly indicated [53–55]. In Figure 11, the temperature dependence of the Leggett mode frequencies is shown for two sets of

values of the intraband scattering lengths: the BCS regime for both bands with $1/a_{s,1} = -1$, $1/a_{s,2} = -2$ (Fig. 11a) and the case with $1/a_{s,1} = 0$, $1/a_{s,2} = -1$ (Fig. 11b). In order to see the range for the possible experimental observation of the Leggett mode, twice the order parameter for a "weak" band is plotted in the same figure. The arrows indicate the upper bound temperature T_L for the observation of the Leggett mode, where $\omega_L = 2|\Psi_2|$. At $T > T_L$, the Leggett mode dissipates, and at $T < T_L$ it can be observable. As seen from Figure 11a, this upper bound temperature exists in the BCS regime. For a stronger coupling $1/a_{s,1} = 0$, $1/a_{s,2} = -1$, however, the condition $\omega_L < 2|\Psi_2|$ is fulfilled in the whole range $0 < T < T_c$. We can conclude that the strong-coupling regime is more favorable for the observation of the Leggett mode than the BCS regime. The strong-coupling regime has been experimentally realized in the condensed atomic gases using the Feshbach resonance. Therefore the observation of the Leggett mode in ultracold Fermi gases is expectable.

4 Conclusions

The first main result of the present work is the derivation of a finite temperature, all-coupling effective field theory for superfluid Fermi gases, obtained by performing a gradient expansion of the pair field around a background value that is not necessarily small. Assuming the validity of the derivative expansion for the order parameter, the effective field action functional has been obtained by systematically summing *all* terms in powers of the order parameter, and is therefore valid at all temperatures below T_c. The expansion has been performed up to second order in both spatial gradients and time derivatives, so that the resulting effective field theory is capable of describing collective excitations for temperatures below T_c. The finite-temperature EFT is a straightforward extension of several preceding approaches: the effective field theory developed for $T \approx T_c$ [11,12] and that developed for $T = 0$ [29,30]. The current formalism corresponds with these approaches in the appropriate limiting cases. Also we retrieve the BCS-BEC theory result for the ground state energy at $T = 0$. Finally, the results for vortices (described here) and for solitons (described in Ref. [31]) correspond well with the results obtained from Bogoliubov-de Gennes calculations. The advantage of the current formalism is that the coefficients of the proposed action functional (54) are closed and tractable expressions, which turn to the known GL coefficients in the limit $T \to T_c$, and are fast to compute.

The present EFT describes the ultracold Fermi gases in the BCS-BEC crossover, smoothly passing the unitarity regime, similarly to reference [11] and the related analytic theories. The unitarity regime needs however a special care, as discussed in Section 2. Accurate quantitative results have been obtained at unitarity and $T = T_c$ using numeric approaches [58,59], and analytically, using different methods, e.g. ε-expansion [60], $1/N$-expansion [61], the renormalization group methods [62–64]. However, these analytic methods are focused at the unitatity regime. At present, to the best of our knowledge, there is no known analytic theory which accurately quantitatively describes the Fermi gases in a unified way through the whole BCS-BEC crossover, including the unitarity point. Therefore the analytic theories smoothly describing the ultracold Fermi gases in the BCS-BEC crossover are useful, because they can provide a reasonable description of ultracold Fermi gases in the whole range of the coupling strength, except the aforesaid singularity point.

It is established in reference [11] that the solution for the critical temperature obtained within the functional integral method accounting for Gaussian fluctuations about the saddle point smoothly interpolates between the two limiting cases – BCS and BEC regimes. Many subsequent works use analytic approximations similar to that in reference [11] for the thermodynamic functions of ultracold Fermi gases (e.g. [12,46,65]). Also our work follows this direction, being particularly aimed on the treatment of the ultracold Fermi gases below T_c.

The second main result of this work is the extension of the effective field formalism to the case of two-band fermionic superfluids. The resulting effective field action contains the same input parameters (the scattering lengths and the interband coupling strength) as those in other approaches to the two-band superfluidity/superconductivity (e.g. Refs. [1,8–10,13]). These input parameters can be independently measured and even precisely controlled – for ultracold gases. They completely fix the microscopic Hamiltonian for the mixture of two atomic Fermi superfluids, with Cooper pairing within each superfluid and contact interactions between the atoms belonging to different superfluids. In the effective bosonic action obtained by the path-integral treatment of this Hamiltonian, the two superfluid order parameters are coupled by a Josephson term that is not introduced ad hoc, but follows directly from applying the Hubbard-Stratonovich transformation, before any approximation is made. This Josephson coupling is kept also after performing the gradient expansion which results in the effective two-field theory.

For the two-band superfluid, the current theory reveals a non-monotonic temperature behavior of the thermodynamic parameters near the (uncoupled) critical temperature of a "weaker" band, similar to that obtained for two-band superconductors with a Bogoliubov-de Gennes treatment (whereas the standard Ginzburg-Landau treatment fails to reproduce this). Also the existence of two healing length scales is captured by the present effective field theory for a two-band Fermi superfluid.

The formalism developed here can find a broad spectrum of applications, in particular as a complementary method to the Bogoliubov-de Gennes equations which are restricted to the mean-field approximation and to the BCS case, and which become cumbersome when many vortices are present. The present method is applicable in the whole range of the BCS-BEC crossover, allows one to take into account the fluctuations, and requires much less computation time than the Bogoliubov-de Gennes formalism. Moreover, the EFT allows one to obtain analytical

solutions in some cases where the Bogoliubov-de Gennes equations can be solved only numerically.

The authors gratefully acknowledge support of the Research Fund of the University of Antwerp. This work was supported by FWO-V projects G.0429.15N, G.0370.09N, G.0180.09N, G.0115.12N, G.0119.12N, the WOG WO.033.09N (Belgium).

Appendix: Effective bosonic action for a two-band system

The integration over the fermionic variables in (45) is performed exactly. We use the Nambu representation with four-dimensional spinors

$$\psi = \begin{pmatrix} \psi_{1,\uparrow} \\ \bar{\psi}_{1,\downarrow} \\ \psi_{2,\downarrow} \\ \bar{\psi}_{2,\uparrow} \end{pmatrix}. \tag{A.1}$$

Note that for the second band we use spin projections opposite to those used in the first band. The HS action (46) is then represented in matrix form as follows:

$$S_{HS} = S_B + S_\chi + \frac{1}{2}\int_0^\beta d\tau \int d\mathbf{r} \begin{pmatrix} \psi & \bar{\psi} \end{pmatrix} \times \begin{pmatrix} \left(-\mathbb{G}^{-1}\right)_{1,1} & \left(-\mathbb{G}^{-1}\right)_{1,2} \\ \left(-\mathbb{G}^{-1}\right)_{2,1} & \left(-\mathbb{G}^{-1}\right)_{2,2} \end{pmatrix} \begin{pmatrix} \psi \\ \bar{\psi} \end{pmatrix}, \tag{A.2}$$

with S_B and S_χ given by (47) and (48), respectively. The following matrices for the inverse 4-dimensional Nambu tensor are introduced:

$$\left(-\mathbb{G}^{-1}\right)_{1,1} = \begin{pmatrix} 0 & 0 & 0 & -i\chi_2 \\ 0 & 0 & i\chi_2 & 0 \\ 0 & -i\chi_2 & 0 & 0 \\ i\chi_2 & 0 & 0 & 0 \end{pmatrix}, \tag{A.3}$$

$$\left(-\mathbb{G}^{-1}\right)_{1,2} = \begin{pmatrix} \frac{\partial}{\partial\tau} - \hat{H}_1 & \bar{\Psi}_1 & -i\chi_1 & 0 \\ \Psi_1 & \frac{\partial}{\partial\tau} + \hat{H}_1 & 0 & i\chi_1 \\ -i\bar{\chi}_1 & 0 & \frac{\partial}{\partial\tau} - \hat{H}_2 & -\bar{\Psi}_2 \\ 0 & i\bar{\chi}_1 & -\Psi_2 & \frac{\partial}{\partial\tau} + \hat{H}_2 \end{pmatrix}, \tag{A.4}$$

$$\left(-\mathbb{G}^{-1}\right)_{2,1} = \begin{pmatrix} \frac{\partial}{\partial\tau} + \hat{H}_1 & -\Psi_1 & i\bar{\chi}_1 & 0 \\ -\bar{\Psi}_1 & \frac{\partial}{\partial\tau} - \hat{H}_1 & 0 & -i\bar{\chi}_1 \\ i\chi_1 & 0 & \frac{\partial}{\partial\tau} + \hat{H}_2 & \Psi_2 \\ 0 & -i\chi_1 & \bar{\Psi}_2 & \frac{\partial}{\partial\tau} - \hat{H}_2 \end{pmatrix}, \tag{A.5}$$

$$\left(-\mathbb{G}^{-1}\right)_{2,2} = \begin{pmatrix} 0 & 0 & 0 & i\bar{\chi}_2 \\ 0 & 0 & -i\bar{\chi}_2 & 0 \\ 0 & i\bar{\chi}_2 & 0 & 0 \\ -i\bar{\chi}_2 & 0 & 0 & 0 \end{pmatrix}. \tag{A.6}$$

The integration over the fermion fields ψ is performed in the same way as in reference [11] and results in a partition function written as a the path integral over the boson fields Ψ and χ,

$$\mathcal{Z} \propto \int \mathcal{D}\left[\bar{\Psi}, \Psi\right] \int \mathcal{D}\left[\bar{\chi}, \chi\right] e^{-S_{\text{eff}}}, \tag{A.7}$$

where the effective bosonic action depends on the pair and density fields through

$$S_{\text{eff}} = S_B - \sum_{j=1,2} \text{Tr} \ln\left[-\mathbb{G}_j^{-1}\right]. \tag{A.8}$$

References

1. H. Suhl, B.T. Matthias, L.R. Walker, Phys. Rev. Lett. **3**, 552 (1959)
2. J. Nagamatsu, N. Nakagawa, T. Muranaka, Y. Zenitani, J. Akimitsu, Nature **410**, 63 (2001)
3. A.Y. Liu, I.I. Mazin, Jens Kortus, Phys. Rev. Lett. **87**, 087005 (2001)
4. Y. Kamihara, T. Watanabe, M. Hirano, H. Hosono, J. Am. Chem. Soc. **128**, 10012 (2006)
5. V.V. Moshchalkov, M. Menghini, T. Nishio, Q.H. Chen, A.V. Silhanek, V.H. Dao, L.F. Chibotaru, N.D. Zhigadlo, J. Karpinski, Phys. Rev. Lett. **102**, 117001 (2009)
6. J. Gutierrez, B. Raes, A.V. Silhanek, L.J. Li, N.D. Zhigadlo, J. Karpinski, J. Tempere, V.V. Moshchalkov, Phys. Rev. B **85**, 094511 (2012)
7. E. Babaev, A. Sudbo, N.W. Ashcroft, Nature **431**, 666 (2004)
8. M. Iskin, C.A.R. Sá de Melo, Phys. Rev. B **72**, 024512 (2005)
9. M. Iskin, C.A.R. Sá de Melo, Phys. Rev. B **74**, 144517 (2006)
10. M. Iskin, C.A.R. Sá de Melo, Phys. Rev. Lett. **97**, 100404 (2006)
11. C.A.R. Sá de Melo, M. Randeria, J.R. Engelbrecht, Phys. Rev. Lett. **71**, 3202 (1993)
12. K. Huang, Z.-Q. Yu, L. Yin, Phys. Rev. A **79**, 053602 (2009)
13. M.E. Zhitomirsky, V.-H. Dao, Phys. Rev. B **69**, 054508 (2004)
14. E. Babaev, M. Speight, Phys. Rev. B **72**, 180502 (2005)
15. A. Gurevich, Phys. Rev. B **67**, 184515 (2003)
16. E. Babaev, J. Carlstrom, M. Speight, Phys. Rev. Lett. **105**, 067003 (2010)
17. V.G. Kogan, J. Schmalian, Phys. Rev. B **83**, 054515 (2011)
18. E. Babaev, M. Silaev, Phys. Rev. B **86**, 016501 (2012)
19. V.G. Kogan, J. Schmalian, Phys. Rev. B **86**, 016502 (2012)
20. A.A. Shanenko, M.V. Milosevic, F.M. Peeters, A.V. Vagov, Phys. Rev. Lett. **106**, 047005 (2011)
21. A. Vagov, A.A. Shanenko, M.V. Milošević, V.M. Axt, F.M. Peeters, Phys. Rev. B **86**, 144514 (2012)
22. M. Silaev, E. Babaev, Phys. Rev. B **84**, 094515 (2011)
23. M. Silaev, E. Babaev, Phys. Rev. B **85**, 134514 (2012)
24. A. Chaves, L. Komendová, M.V. Milošević, J.S. Andrade Jr., G.A. Farias, F.M. Peeters, Phys. Rev. B **83**, 214523 (2011)

25. N.V. Orlova, A.A. Shanenko, M.V. Milošević, F.M. Peeters, A.V. Vagov, V.M. Axt, Phys. Rev. B **87**, 134510 (2013)
26. L. Komendová, M.V. Milošević, A.A. Shanenko, F.M. Peeters, Phys. Rev. B **84**, 064522 (2011)
27. L. Tewordt, Phys. Rev. **132**, 595 (1963)
28. N.R. Werthammer, Phys. Rev. **132**, 663 (1963)
29. M. Marini, F. Pistolesi, G.C. Strinati, Eur. Phys. J. B **1**, 151 (1998)
30. A.M.J. Schakel, Ann. Phys. **326**, 193 (2011)
31. S.N. Klimin, J. Tempere, J.T. Devreese, Phys. Rev. A **90**, 053613 (2014)
32. E. Babaev, H. Kleinert, Phys. Rev. B **59**, 12083 (1999)
33. S.S. Botelho, C.A.R. Sá de Melo, Phys. Rev. Lett. **96**, 040404 (2006)
34. J.-T. Hsiang, C.-Y. Lin, D.-S. Lee, R.J. Rivers, J. Phys.: Condens. Matter **25**, 404211 (2013)
35. E. Taylor, A. Griffin, Y. Ohashi, Phys. Rev. A **76**, 023614 (2007)
36. E. Abrahams, T. Tsuneto, Phys. Rev. **152**, 416 (1966)
37. L.P. Gorkov, G.M. Eliashberg, Zh. Eksp. Teor. Fiz. **54**, 612 (1968) [Sov. Phys. J. Exp. Theor. Phys. **27**, 328 (1968)]
38. H. Ebisawa, H. Fukuyama, Prog. Theor. Phys. **46**, 1042 (1971)
39. M. Machida, T. Koyama, Phys. Rev. A **74**, 033603 (2006)
40. Y.E. Kim, A.L. Zubarev, Phys. Rev. A **70**, 033612 (2004)
41. N. Manini, L. Salasnich, Phys. Rev. A **71**, 033625 (2005)
42. S. Simonucci, P. Pieri, G.C. Strinati, Phys. Rev. B **87**, 214507 (2013)
43. E. Taylor, A. Griffin, N. Fukushima, Y. Ohashi, Phys. Rev. A **74**, 063626 (2006)
44. J. Tempere, S.N. Klimin, J.T. Devreese, Phys. Rev. A **79**, 053637 (2009)
45. S. Simonucci, G.C. Strinati, Phys. Rev. B **89**, 054511 (2014)
46. R.B. Diener, R. Sensarma, M. Randeria, Phys. Rev. A **77**, 023626 (2008)
47. S.N. Klimin, J.T. Devreese, J. Tempere, New J. Phys. **14**, 103044 (2012)
48. L. Salasnich, P.A. Marchetti, F. Toigo, Phys. Rev. A **88**, 053612 (2013)
49. H. Kleinert, Electronic J. Theor. Phys. **8**, 57 (2011)
50. L. Komendová, Y. Chen, A.A. Shanenko, M.V. Milosevic, F.M. Peeters, Phys. Rev. Lett. **108**, 207002 (2012)
51. F. Palestini, G.C. Strinati, Phys. Rev. B **89**, 224508 (2014)
52. A.J. Leggett, Prog. Theor. Phys. **36**, 901 (1966)
53. G. Blumberg, A. Mialitsin, B.S. Dennis, M.V. Klein, N.D. Zhigadlo, J. Karpinski, Phys. Rev. Lett. **99**, 227002 (2007)
54. Ya.G. Ponomarev et al., Solid State Commun. **129**, 85 (2004)
55. E.G. Maksimov, A.E. Karakozov, B.P. Gorshunov, Ya.G. Ponomarev, E.S. Zhukova, M. Dressel, J. Exp. Theor. Phys. **115**, 252 (2012)
56. M. Ichioka, Progr. Theor. Phys. **90**, 513 (1993)
57. S.G. Sharapov, V.P. Gusynin, H. Beck, Eur. Phys. J. B **30**, 45 (2002)
58. A. Bulgac, J.E. Drut, P. Magierski, Phys. Rev. Lett. **96**, 090404 (2006)
59. E. Burovski, N. Prokof'ev, B. Svistunov, M. Troyer, Phys. Rev. Lett. **96**, 160402 (2006)
60. Y. Nishida, D.T. Son, Phys. Rev. Lett. **97**, 050403 (2006)
61. T. Enss, Phys. Rev. A **86**, 013616 (2012)
62. P. Nikolić, S. Sachdev, Phys. Rev. A **75**, 033608 (2007)
63. K.B. Gubbels, H.T.C. Stoof, Phys. Rev. Lett. **100**, 140407 (2008)
64. I. Boettcher, J.M. Pawlowski, C. Wetterich, Phys. Rev. A **89**, 053630 (2014)
65. R. Haussmann, W. Rantner, S. Cerrito, W. Zwerger, Phys. Rev. A **75**, 023610 (2007)